Space debris

Cătălin Galeş

Al. I. Cuza University of Iaşi
Department of Mathematics

Work in collaboration with Alessandra Celletti from University of Rome Tor Vergata.

I-CELMECH Training School, February 3-7, 2020

February 6, 2020

Outline

1. Introduction
1.1 Origin of space debris
1.2 Breakup events
1.3 The circumterrestrial space
1.4 The LEO environment
1.5 Space debris mitigation strategies

2. Formulation of the problem
2.1 Equations of motion in Cartesian coordinates
2.2 Hamiltonian approach
2.3 Effects of J_2

3. Tesseral resonances
3.1 Tesseral resonances in GEO and MEO
3.2 Tesseral resonances in the LEO region

4. Lunisolar resonances
4.1 Semi–secular resonances
4.2 Secular resonances

5. Conclusions and perspectives

Outline

1. Introduction
1.1 Origin of space debris
1.2 Breakup events
1.3 The circumterrestrial space
1.4 The LEO environment
1.5 Space debris mitigation strategies

2. Formulation of the problem
2.1 Equations of motion in Cartesian coordinates
2.2 Hamiltonian approach
2.3 Effects of J_2

3. Tesseral resonances
3.1 Tesseral resonances in GEO and MEO
3.2 Tesseral resonances in the LEO region

4. Lunisolar resonances
4.1 Semi–secular resonances
4.2 Secular resonances

5. Conclusions and perspectives

Origin of space debris

- Space debris (orbital debris or space junks) are artificial (non-operational or defunct) objects in orbit around the Earth.
- These objects are remnants of space missions, like rocket stages, old satellites, fragments from disintegrations, lost equipment, bolts, paint flakes, batteries, etc.

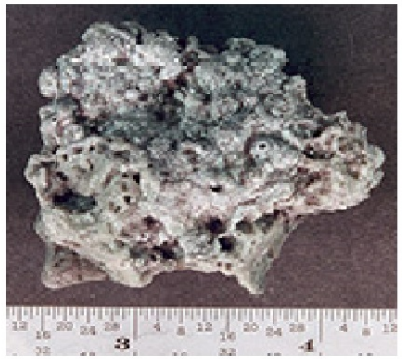

Figure : Left: The main propellant tank of the second stage of a Delta 2 launch vehicle which landed near Georgetown, TX, on 22 January 1997. (Credit: NASA ODPO). Right: Solid rocket motor (SRM) slag. Aluminum oxide slag is a byproduct of SRMs. (Credit: NASA).

• Space debris have been produced in last 60 years as effect of the exploration and exploitation of the circumterrestrial space.

• Space Launch Report archive lists more than 5400 launches since 4th October 1957, which deployed more than 8000 spacecraft and satellites.

• Catastrophic events (explosions and collisions) have dramatically increased the number of objects in orbit.

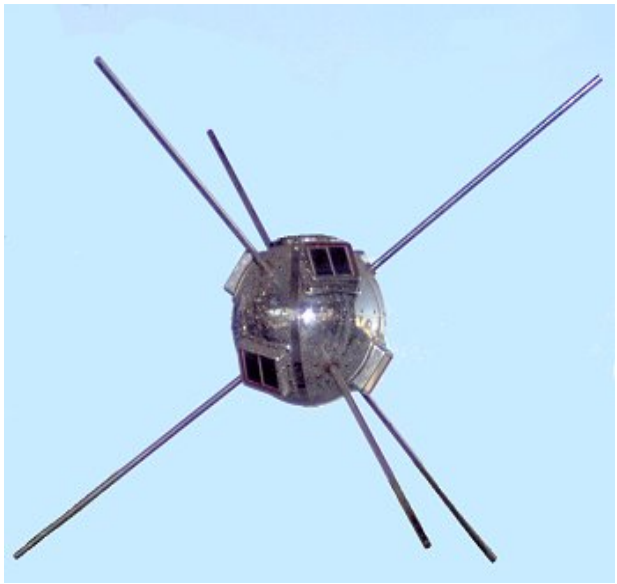

Figure : Vanguard 1 is the first space debris. It was launched on an elliptic orbit on 17 March 1958. Lifetime is estimated at 240 years. (Credit: NASA).

• More than 22300 objects with size larger than 10 *cm* are being regularly tracked by the U.S. Space Surveillance Network, of which approximately 94% are space debris and the rest 6% (around 2000) are operational satellites.

≈ 6% operative satellites; ≈ 24% non–operative satellites;

≈ 17% rocket upper stages; ≈ 53% mission related debris and fragments.

• Estimates: about 34000 objects larger than10 cm, 900, 000 objects larger than1 cm; about 130×10^6 objects larger than 1 mm.

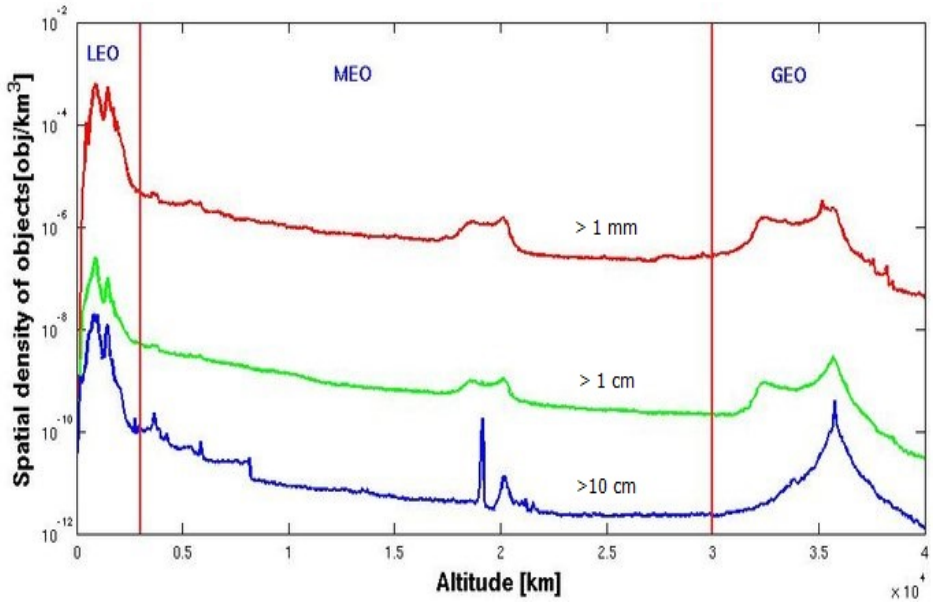

Figure : Spatial density of objects as a function of altitude. (Reproduced from http://www.scholarpedia.org/article/Space debris)

Breakup events

- The large number of fragments is due to explosions and collisions.
- More than 500 confirmed breakups since 1961.
- The cause of explosions is the residual fuel left in tanks and fuel lines or other sources of energy left at the board of the satellite of spacecraft.
- The velocities of the objects in the Earth's orbit are of the order of ($\approx 10\ km/s$).
- A collision with a:
  – 10 cm object would entail a catastrophic fragmentation of a typical satellite;
  – 1 cm object would most likely disable a spacecraft and penetrate the ISS shields;
  – 1 mm object could destroy sub-systems on board a spacecraft.
- 29 June 1961, first explosion in space: Thor-Able upper stage exploded two hours after the separation from the Transit 4A navigation satellite. Number of fragments tracked from the ground: 294.
- 24 July 1996, first accidental collision in space: The 50 kg microsatellite Cerise has been hit by a fragment coming from the explosion of the rocket Ariane.
- The most famous events are the breakup of the Fengyun–1C satellite in 2007 (more than 3700 fragments) and the collision of the Cosmos 2251 and the Iridium 33 spacecraft in 2009 (more than 1700 fragments).

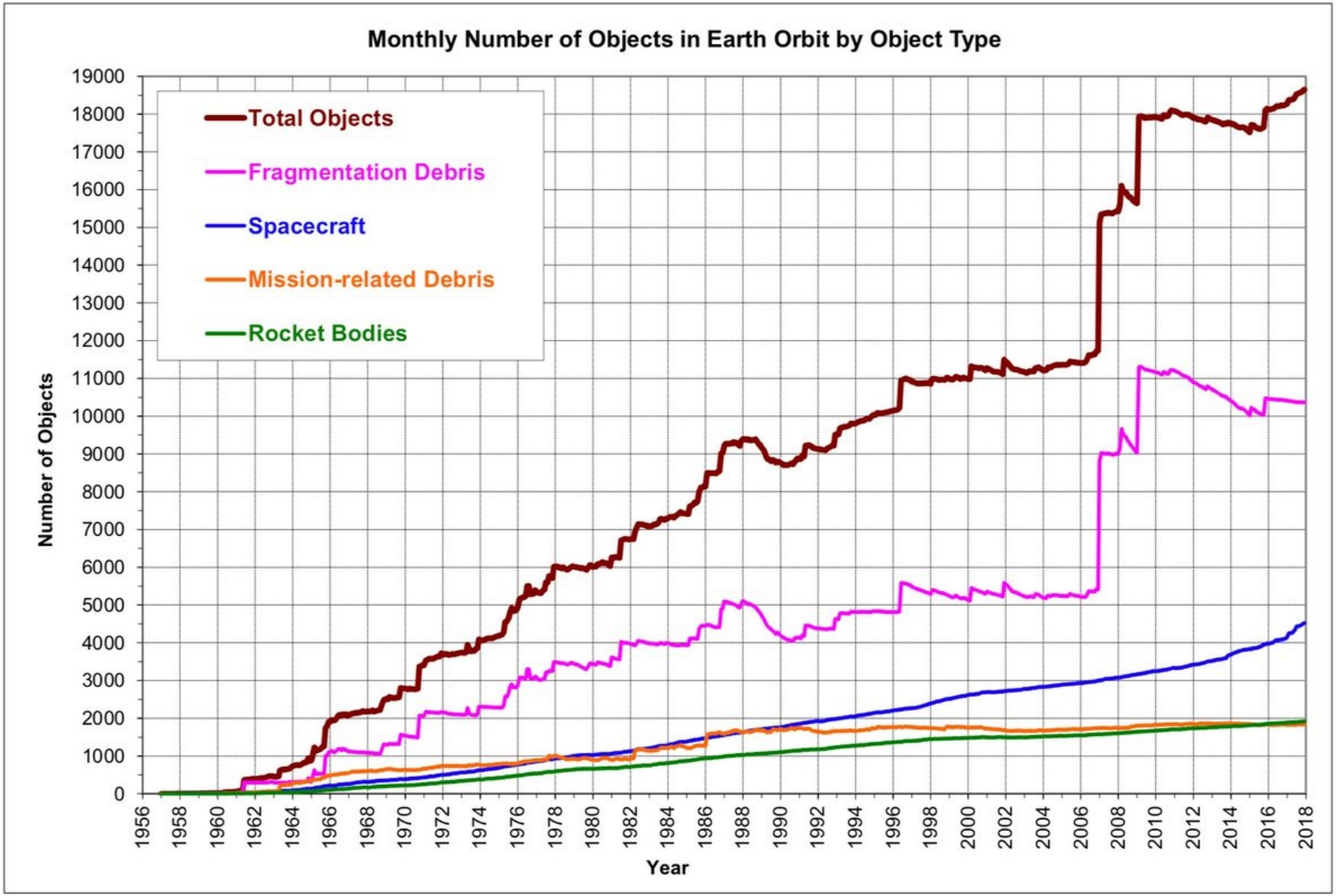

Figure : Growth of the number of objects in space (reproduced from http://www.jaxa.jp)

• Each time an object breaks up, whether by collision or explosion, a debris cloud is formed.

• The spatial density of debris with respect to the background flux increases considerable. There are possible other collisions.

• The scientific community worries that the Kessler syndrome (in which the density of objects is high enough that collisions between objects lead to a cascade effect) has already begun in the LEO region.

• The Inter-Agency Space Debris Coordination Committee (IADC), founded in 1993, is an international forum of governmental bodies for the coordination of activities related to the issues of man-made and natural debris in space.
– exchange information on space debris research activities between member space agencies;
– facilitate opportunities for co-operation in space debris research;
– review the progress of ongoing co-operative activities;
– identify debris mitigation options.

The circumterrestrial space

- The circumterrestrial space is divided into the following regions:

–LEO (low-Earth orbit), running from 0 to 2,000 km in altitude;

–MEO (medium-Earth orbit), the region between 2,000 and 30,000 km in altitude;

–GEO (geostationary-Earth orbit), trajectories around the altitude of 35,786 km;

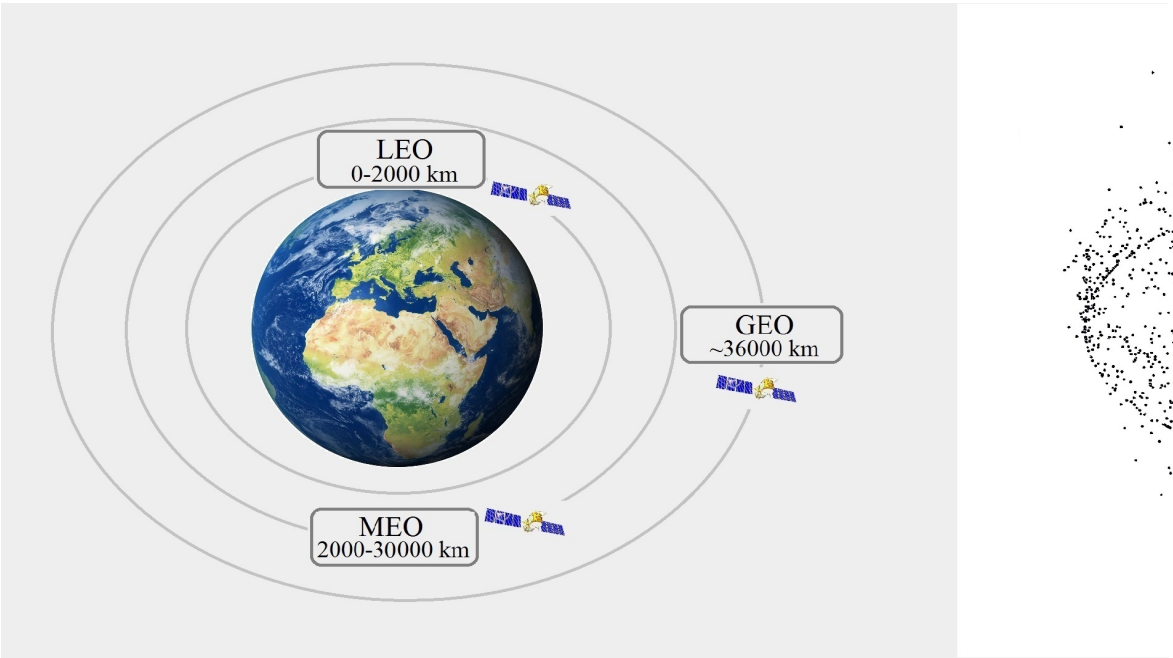

Figure : Left: The circumterrestrial space; Right: Satellites and space debris (Courtesy NASA).

• PHYSICS

◇ Conservative regime in MEO, GEO Regions affected by the monopole term of the Earth's attraction, Earth's oblateness J_2 and J_{22}, attraction of the Moon, influence of the Sun and SRP.

◇ Dissipative regime in LEO. Region affected also by the atmospheric drag.

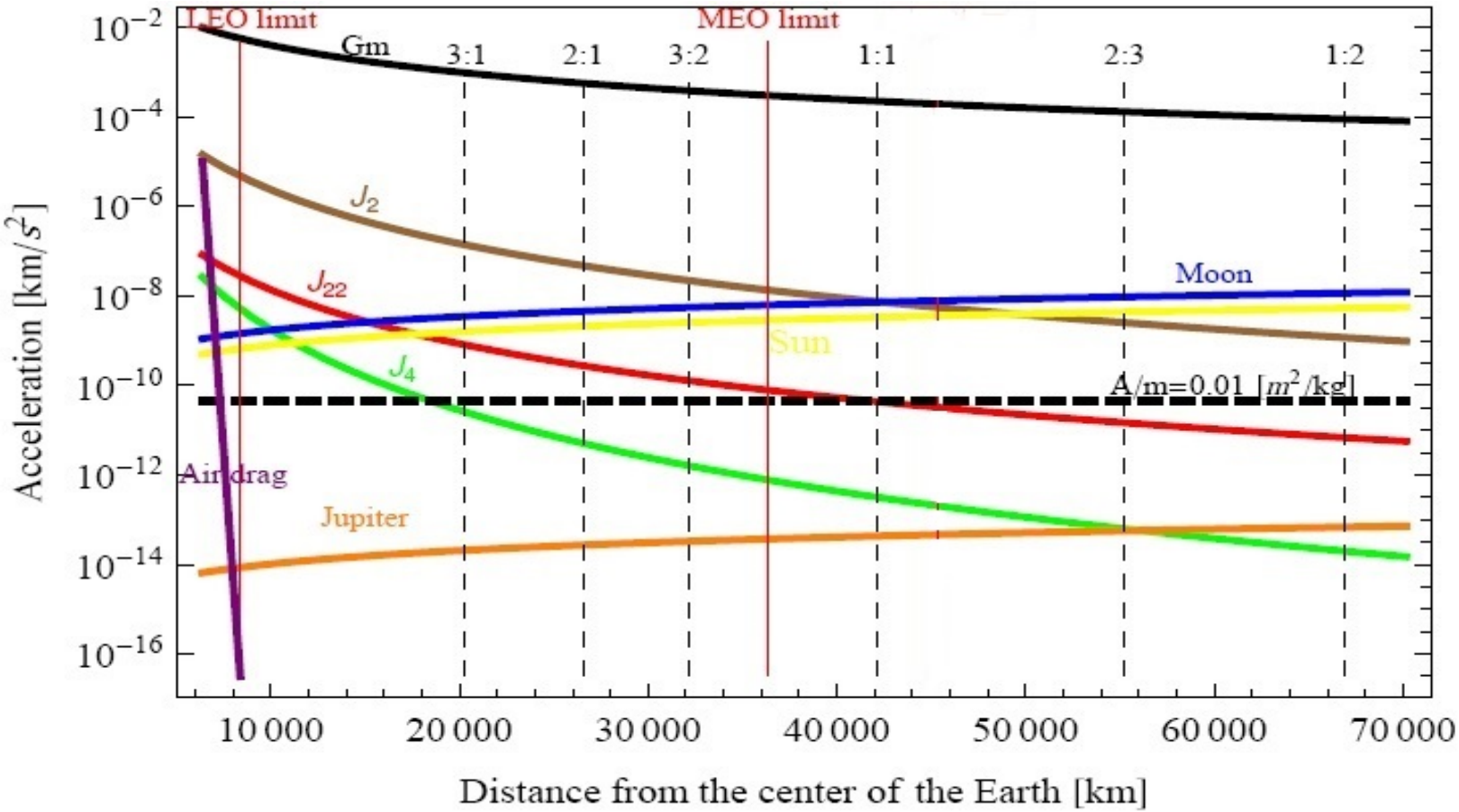

Figure : Order of magnitude of various perturbations of a satellite orbit.

• DYNAMICS

The long-term evolution of satellite orbits depends on various effects:

◇ **A) Gravitational resonances**

–**Tesseral resonances** occur whenever there is a commensurability between the orbital period of a satellite and the period of Earth's rotation. Main effect: a variation of the semi-major axis on time scales of the order of hundred of days (see Breiter (2005), Valk et al. (2009), Celletti et al. (2014, 2015))

–**Lunisolar resonances** involve commensurabilities between slow angles: ω, Ω, ω_M, Ω_M, M_S. Main effect: variations of eccentricity and inclination on time scales of the order to tens (or hundred) of years. (see Rosengren et al. (2015), Daquin et al. (2016), Alessi et al. (2016), Celletti et al. (2016, 2017), Gkolias et al. (2019).

◇ **B) Solar radiation pressure** influences the orbits of high area-to-mass ratio objects (HAMR). Main effects: periodic motion of the orbital elements; in particular annual periodic motion of the eccentricity (see Valk et al. (2008, 2009)). **Secondary resonances** involving and the Sun's longitude (see Lemaître et al. (2009)).

◇ **C) Dissipation.** Different atmospheric models give different results (see Petit and Lemaitre (2017)); Combined effect of air drag and resonances (tesseral or lunisolar) have been addressed recently (Celletti and CG (2018), Alessi et al. (2018)).

◇ **D)** Various **dynamical phenomena** like overlapping of resonances (tesseral or secular) and the onset of chaos (see Celletti et al. (2014–2017), Rosengren et al. (2015), Daquin et al. (2016)), bifurcations of equilibria Celletti et al. (2016,2017), interplay between conservative and dissipative effects (Celletti and CG (2018)), etc.

The LEO environment

- Space assets are constantly hit by high–speed micrometeoroids ($\approx 20\ km/s$) and debris ($\approx 10\ km/s$).
- In LEO, the debris population dominates the micrometeoroid population for objects greater than 1 mm. For particles less than 1 mm, the two populations are equal.

The LEO environment

• Space assets are constantly hit by high–speed micrometeoroids ($\approx 20\ km/s$) and debris ($\approx 10\ km/s$).
• In LEO, the debris population dominates the micrometeoroid population for objects greater than 1 *mm*. For particles less than 1 *mm*, the two populations are equal.
• According to the NASA Johnson Space Center's Hypervelocity Impact Technology Facility, in 64 missions (from STS–50 through STS–114):
– the Shuttle's windows have been hit 1634 times necessitating 92 window replacements;
– the Shuttle's radiator was hit 317 times, actually causing holes in the radiator's facesheet 53 times.

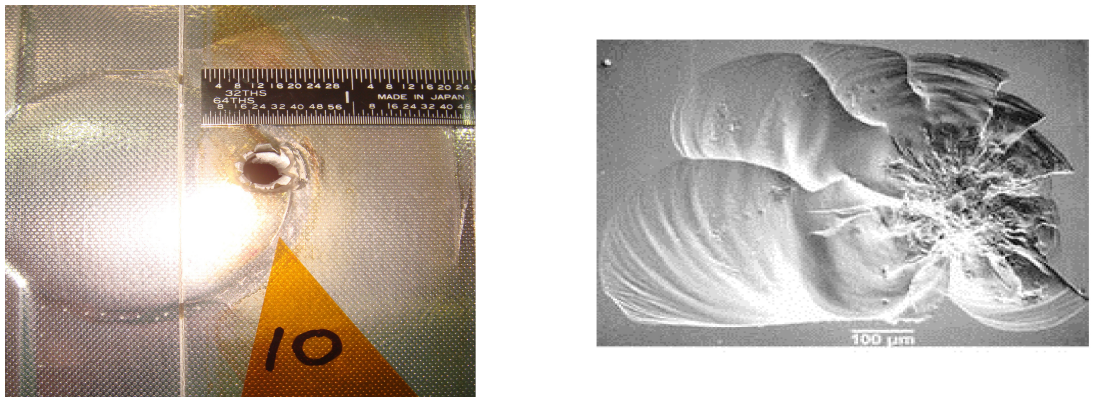

Figure : Left: Hypervelocity impact of the radiator panel LH4 of the Columbia space shuttle STS-118 (the hole is about 5.54 mm). Right: Impact crater on window number 6 of the Columbia space shuttle STS-50 caused by a solid rocket motor particle. (Courtesy NASA)

• The Astromaterials Acquisition and Curation Office at the Johnson Space Center curates all of NASA's astromaterials samples. Since 1985, a large variety of space-exposed materials from spacecraft and satellites have been selected and curated.
• The current sources of these harvested materials are: Long Duration Exposure Facility (LDEF); Solar Maximum Satellite (SolarMax); European Recoverable Carrier (EURECA); Hardware from the Hubble Space Telescope, etc.

• The Astromaterials Acquisition and Curation Office at the Johnson Space Center curates all of NASA's astromaterials samples. Since 1985, a large variety of space-exposed materials from spacecraft and satellites have been selected and curated.
• The current sources of these harvested materials are: Long Duration Exposure Facility (LDEF); Solar Maximum Satellite (SolarMax); European Recoverable Carrier (EURECA); Hardware from the Hubble Space Telescope, etc.
• LDEF was deployed in orbit on April 7, 1984 at an altitude of 475 km and inclination of 28.4^o, and retrieved on January 11, 1990 (5.7 years in space).
• LDEF provided a unique source of information concerning the LEO environment. One has scanned 48 frame components (i.e. intercostals) from LDEF, about 2.8 m^2 of the surface. Results: 7237 craters larger than 10 μm, from which 10 are about 0.1 cm.

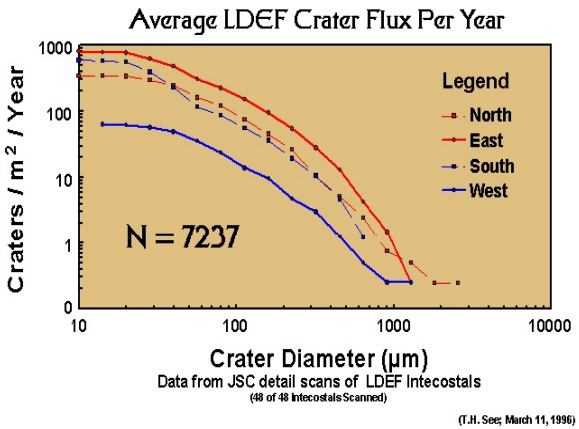

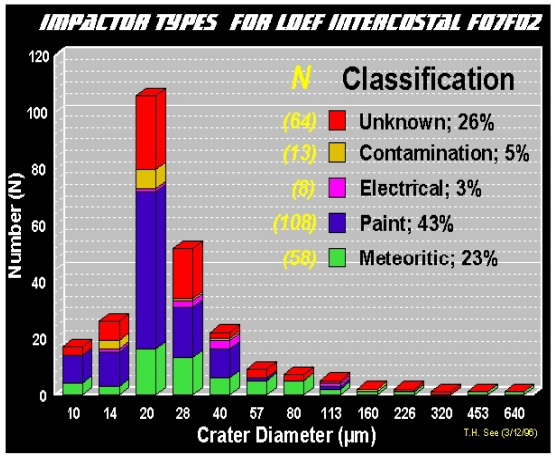

Figure : Left: LDEF; Middle: Average LDEF crater flux per year; Right: Impactor types. (Courtesy NASA)

Space debris mitigation strategies

- To stabilize the space debris population growth, IADC adopted a set of guidelines which are based on the following general principles:

– preventing on-orbit break-ups;

– removing spacecraft and orbital stages that have reached the end of their mission operations from the useful densely populated orbit regions;

– limiting the objects released during normal operations.

- Two protected regions about the Earth:

A) The Low Earth orbit (LEO); B) The geosynchronous orbit (GEO) protected region: the space bounded in altitude by $\pm\Delta H$ km of the geosynchronous altitude (35786 km) and in inclination by $\pm 15^o$.

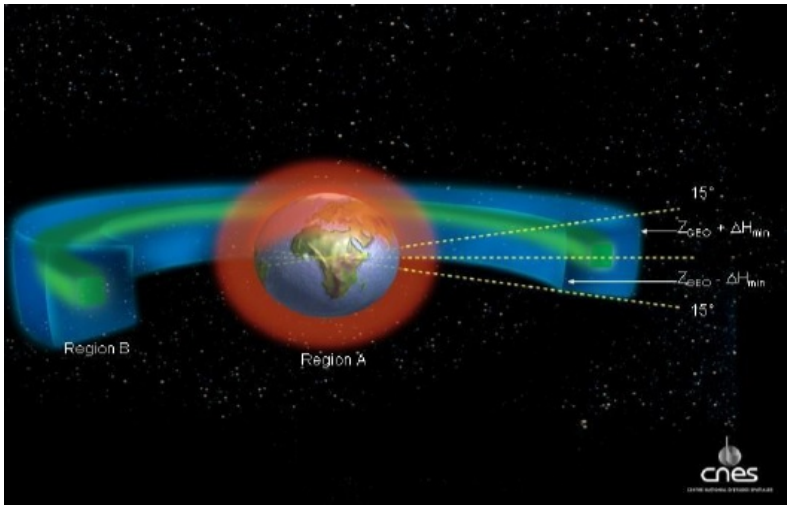

Figure : Protected regions (Reproduced from the IADC Assessment Report for 2010.

• For LEO and GEO, the mitigation measures proposed by Inter-Agency Space Debris Coordination Committee (IADC) are able to strongly reduce the growth of the number of objects.
• In LEO, the orbital life time could vary from months to centuries. For an object with a large ballistic coefficient, say $B = 200\ cm^2/kg$, the orbital lifetime is: 1 *month* at 300 *km*, 1 *year* at 400 *km*, *decades* at 800 *km* and *centuries* at altitudes larger than 900 *km*.
• Mitigation strategies in LEO: the space systems interfering with the LEO region should be de-orbited (direct re-entry is preferred), or manoeuvred into an orbit with a reduced lifetime. Retrieval is also a disposal option. Some IADC and other studies have found 25 years to be a reasonable and appropriate lifetime limit.

• For LEO and GEO, the mitigation measures proposed by Inter-Agency Space Debris Coordination Committee (IADC) are able to strongly reduce the growth of the number of objects.
• In LEO, the orbital life time could vary from months to centuries. For an object with a large ballistic coefficient, say $B = 200\ cm^2/kg$, the orbital lifetime is: 1 *month* at 300 *km*, 1 *year* at 400 *km*, *decades* at 800 *km* and *centuries* at altitudes larger than 900 *km*.
• Mitigation strategies in LEO: the space systems interfering with the LEO region should be de-orbited (direct re-entry is preferred), or manoeuvred into an orbit with a reduced lifetime. Retrieval is also a disposal option. Some IADC and other studies have found 25 years to be a reasonable and appropriate lifetime limit.
• For the GEO case, spacecraft at end-of-life should be moved to a disposal orbits with the perigee higher than the geostationary altitude by an amount $\Delta H(km)$ given by

$$\Delta H = 235 + C_r\, 1000\, A/m$$

where A/m is the area–to–mass ratio, while C_r is radiation pressure coefficient, typically between 1 and 2, which specifies the amount of solar radiation transmitted, absorbed and reflected by the spacecraft.

- There are no internationally agreed mitigation guidelines in MEO.

- There are no internationally agreed mitigation guidelines in MEO.
- Orbital elements and constellation size of the global navigation satellite systems (GNSS):

-GPS (American): $a = 26\,560\,km$, $i = 55^o$, $e \simeq 0$; Constellation size: 32, In orbit: 31;

-GLONASS (Russian): $a = 25\,440\,km$, $i = 64^o$, $e \simeq 0$; Size: 26, In orbit: 24;

-Galileo (European): $a = 29\,600\,km$, $i = 56^o$, $e \simeq 0$; Size: 30, Usable: 22, Testing: 2, Unavailable: 2, Retired: 2

-BeiDou (Chinese): $a = 27\,900\,km$, $i = 55^o$, $e \simeq 0$; Size: 35, In orbit: 24

- There are no internationally agreed mitigation guidelines in MEO.
- Orbital elements and constellation size of the global navigation satellite systems (GNSS):

-GPS (American): $a = 26\,560\,km$, $i = 55^o$, $e \simeq 0$; Constellation size: 32, In orbit: 31;

-GLONASS (Russian): $a = 25\,440\,km$, $i = 64^o$, $e \simeq 0$; Size: 26, In orbit: 24;

-Galileo (European): $a = 29\,600\,km$, $i = 56^o$, $e \simeq 0$; Size: 30, Usable: 22, Testing: 2, Unavailable: 2, Retired: 2

-BeiDou (Chinese): $a = 27\,900\,km$, $i = 55^o$, $e \simeq 0$; Size: 35, In orbit: 24

- Two end-of-life disposal strategies: the graveyard orbit scenario and the eccentricity growth scenario.

• There are no internationally agreed mitigation guidelines in MEO.

• Orbital elements and constellation size of the global navigation satellite systems (GNSS):

-GPS (American): $a = 26\,560\,km$, $i = 55^o$, $e \simeq 0$; Constellation size: 32, In orbit: 31;

-GLONASS (Russian): $a = 25\,440\,km$, $i = 64^o$, $e \simeq 0$; Size: 26, In orbit: 24;

-Galileo (European): $a = 29\,600\,km$, $i = 56^o$, $e \simeq 0$; Size: 30, Usable: 22, Testing: 2, Unavailable: 2, Retired: 2

-BeiDou (Chinese): $a = 27\,900\,km$, $i = 55^o$, $e \simeq 0$; Size: 35, In orbit: 24

• Two end-of-life disposal strategies: the graveyard orbit scenario and the eccentricity growth scenario.

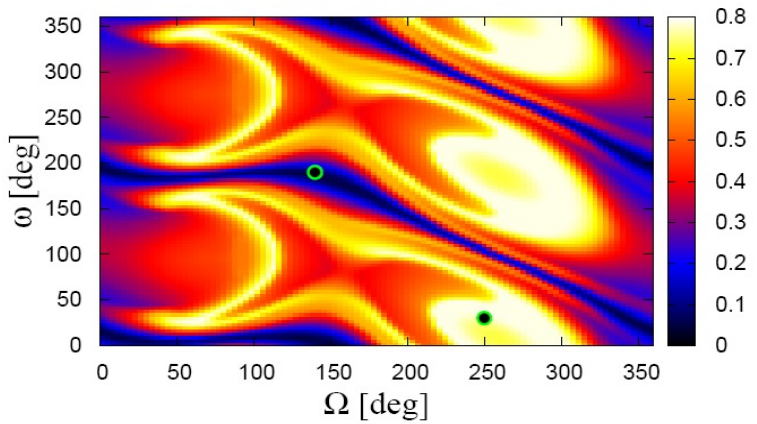

Figure : Maximum eccentricity reached in 200 years (color bar) as a function of ω and Ω. The other initial conditions are $a(0) = 26\,520\,km$, $e(0) = 0.05122$ and $i(0) = 56^o$ at the initial Epoch J2000 (January 1, 2000, 12:00 GMT).

• It is mandatory to understand the dynamics of this population in order devise maintenance and control strategies, as well as mitigation strategies.

• **AIM OF THE LECTURE:** Resonance effects within LEO, MEO and GEO:

tesseral resonances: between debris' orbital period and Earth's rotation

lunisolar secular resonances: between slow angles ω, Ω, ω_M, Ω_M, M_S

interplay between the conservative and dissipative effects in LEO

• **MODELS AND METHODS**: appropriate modeling of the dynamics through

◇ Cartesian equations: include easily all effects, used by space agencies.

◇ Delaunay variables: locate resonances, bifurcations, pendulum-like structure.

• **RESULTS**: qualitative and quantitative study of resonances in GEO, MEO, LEO

I. Tesseral resonances provoke variations of the semi–major axis:

▷ GEO and MEO: a) locate the equilibria and measure the amplitudes of the libration islands; b) bifurcations, overlapping of resonances, chaotic variation of semi-major axis; c) point out the role of zonal and tesseral harmonics.

▷ LEO: a) show the existence of equilibrium points and study the type of equilibria; b orbital decay, caused by the air drag, can be balanced by resonant effects; c) temporary capture or escape from resonance, shifts of equilibria along some axes;

II. Lunisolar resonances influence the evolution of eccentricity and inclination:

▷ bifurcations; libration regions leading to large as well as small excursions in e; eccentricity growth as effect of secular resonances and chaos; overlapping of resonances and the onset of chaos with variation of the orbital elements.

Outline

1. Introduction
1.1 Origin of space debris
1.2 Breakup events
1.3 The circumterrestrial space
1.4 The LEO environment
1.5 Space debris mitigation strategies

2. Formulation of the problem
2.1 Equations of motion in Cartesian coordinates
2.2 Hamiltonian approach
2.3 Effects of J_2

3. Tesseral resonances
3.1 Tesseral resonances in GEO and MEO
3.2 Tesseral resonances in the LEO region

4. Lunisolar resonances
4.1 Semi–secular resonances
4.2 Secular resonances

5. Conclusions and perspectives

Equations of motion in Cartesian coordinates

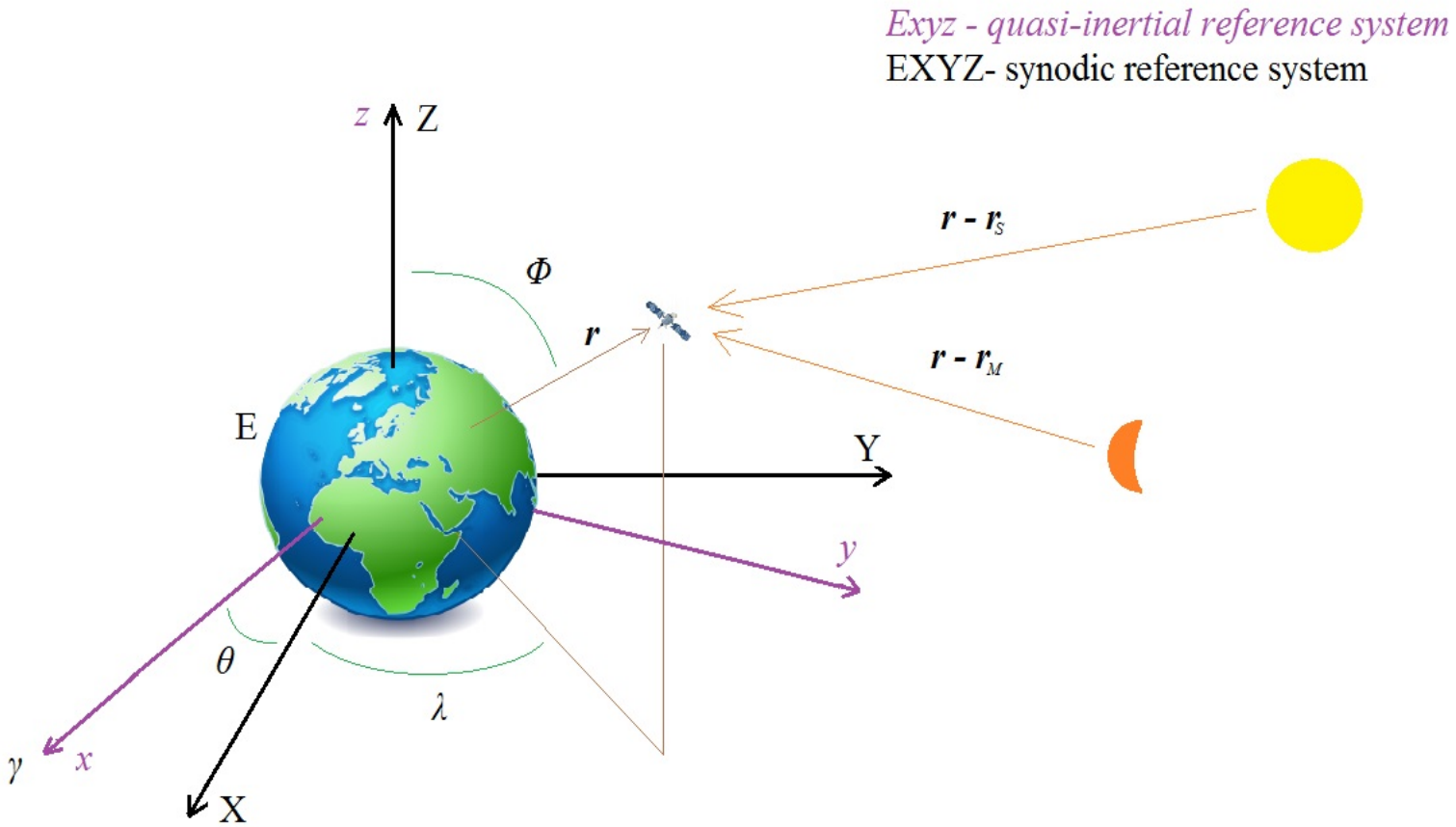

Figure : Quasi–inertial and synodic reference systems.

- The motion is described by:

$$\begin{aligned}\ddot{\mathbf{r}} &= R_3(-\theta)\,\nabla V(\mathbf{r}) - Gm_S\left(\frac{\mathbf{r}-\mathbf{r}_S}{|\mathbf{r}-\mathbf{r}_S|^3}+\frac{\mathbf{r}_S}{|\mathbf{r}_S|^3}\right)\\ &- Gm_M\left(\frac{\mathbf{r}-\mathbf{r}_M}{|\mathbf{r}-\mathbf{r}_M|^3}+\frac{\mathbf{r}_M}{|\mathbf{r}_M|^3}\right)+C_r\,P_r\,a_S^2\,(\frac{A}{m})\,\frac{\mathbf{r}-\mathbf{r}_S}{|\mathbf{r}-\mathbf{r}_S|^3}+\mathbf{a}_{ng}\ , \qquad (1)\end{aligned}$$

- In terms of spherical harmonics, the Earth's gravity potential has the form (Kaula 1966):

$$V(r,\phi,\lambda) = -\sum_{n=0}^{\infty}\sum_{m=0}^{n} V_{nm} = \frac{GM_E}{r}\sum_{n=0}^{\infty}\sum_{m=0}^{n}\left(\frac{R_E}{r}\right)^n P_{nm}(\sin\phi)\,J_{nm}\cos[(m\lambda-\lambda_{nm})]\ ,$$

- The motion is described by:

$$\begin{aligned}\ddot{\mathbf{r}} &= R_3(-\theta)\,\nabla V(\mathbf{r}) - Gm_S\left(\frac{\mathbf{r}-\mathbf{r}_S}{|\mathbf{r}-\mathbf{r}_S|^3}+\frac{\mathbf{r}_S}{|\mathbf{r}_S|^3}\right)\\ &- Gm_M\left(\frac{\mathbf{r}-\mathbf{r}_M}{|\mathbf{r}-\mathbf{r}_M|^3}+\frac{\mathbf{r}_M}{|\mathbf{r}_M|^3}\right)+C_r\,P_r\,a_S^2\,(\frac{A}{m})\,\frac{\mathbf{r}-\mathbf{r}_S}{|\mathbf{r}-\mathbf{r}_S|^3}+\mathbf{a}_{ng}\ , \qquad (1)\end{aligned}$$

- In terms of spherical harmonics, the Earth's gravity potential has the form (Kaula 1966):

$$V(r,\phi,\lambda) = -\sum_{n=0}^{\infty}\sum_{m=0}^{n} V_{nm} = \frac{GM_E}{r}\sum_{n=0}^{\infty}\sum_{m=0}^{n}\left(\frac{R_E}{r}\right)^n P_{nm}(\sin\phi)\,J_{nm}\cos[(m\lambda-\lambda_{nm})]\ ,$$

- The fast Lyapunov indicator (hereafter FLI), (see (C. Froeschlé et al. 1997, Guzzo et al. 2002, 2013) defined as:

$$FLI(\mathfrak{X}(0),\mathcal{V}(0),T) \equiv \sup_{0<t\leq T}\log||\mathcal{V}(t)||\ .$$

for an initial condition $\mathfrak{X}(0)$ at a time $t=T$, provides information on the regular or chaotic character of the dynamics, the location of the equilibrium points, the role of higher degree harmonic terms. Here, $\mathfrak{X}$ is the state of the system and $\mathcal{V}$ is the tangent vector.

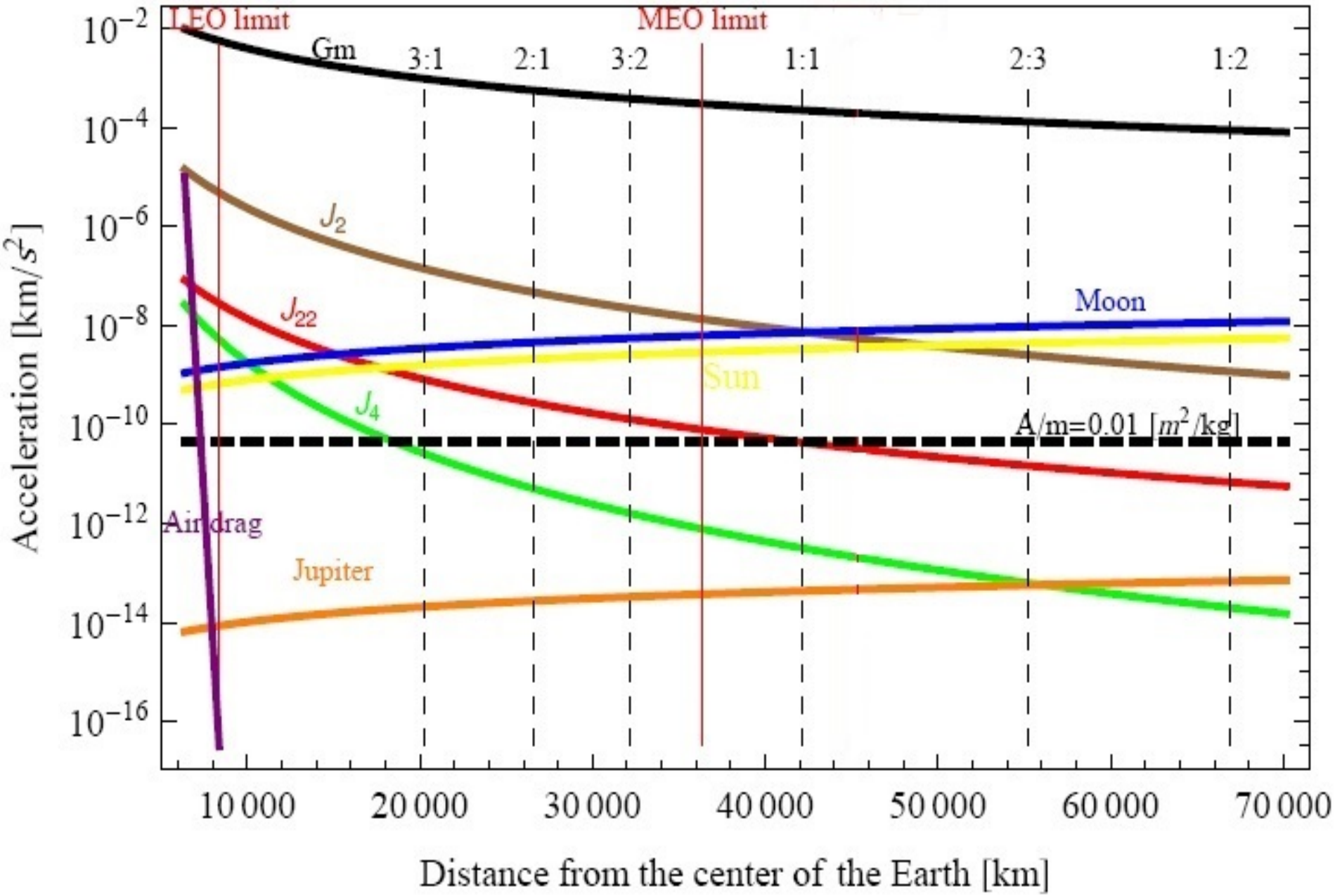

Figure : Order of magnitude of various perturbations of a space debris orbit.

Delaunay variables

• The action–angle Delaunay variables $(L, G, H, M, \omega, \Omega)$ are related to the orbital elements $(a, e, i, M, \omega, \Omega)$ by

$$L = \sqrt{\mu_E a}\,, \qquad G = L\sqrt{1-e^2}\,, \qquad H = G\cos i\,.$$

The dynamical equations of motion are given by

$$\dot{M} = \frac{\partial \mathcal{H}}{\partial L}\,, \qquad \dot{\omega} = \frac{\partial \mathcal{H}}{\partial G}\,, \qquad \dot{\Omega} = \frac{\partial \mathcal{H}}{\partial H}$$

$$\dot{L} = -\frac{\partial \mathcal{H}}{\partial M} + F_L\,, \qquad \dot{G} = -\frac{\partial \mathcal{H}}{\partial \omega} + F_G\,, \qquad \dot{H} = -\frac{\partial \mathcal{H}}{\partial \Omega} + F_H\,,$$

where the conservative part is described by the Hamiltonian

$$\mathcal{H} = -\frac{\mu_E^2}{2L^2} + \mathcal{H}_{Earth}(a, e, i, M, \omega, \Omega, \theta) + \mathcal{H}_{Moon}(a, e, i, M, \omega, \Omega, \Lambda_M)$$
$$+\mathcal{H}_{Sun}(a, e, i, M, \omega, \Omega, \Lambda_S) + \mathcal{H}_{SRP}(a, e, i, M, \omega, \Omega, \Lambda_S)\,.$$

with $\mu_E = \mathcal{G}\, m_E$, θ sidereal time, Λ_M, Λ_S = orbital elements of Moon w.r.t. ecliptic and Sun w.r.t. celestial equator, while F_L, F_G, F_H are the components of the dissipative effects due to the atmospheric drag.

Conservative part

- The Fourier expansion of $\mathcal{H}_{Earth}$ has the form (Kaula 1966, Chao 2005):

$$\mathcal{H}_{Earth} = \frac{\mu_E}{a} \sum_{n=2}^{\infty} \sum_{m=0}^{n} \left(\frac{R_E}{a}\right)^n J_{nm} \sum_{p=0}^{n} F_{nmp}(i) \sum_{q=-\infty}^{\infty} G_{npq}(e)\, cs_{nm}\Big(\Psi_{nmpq}(M,\omega,\Omega,\theta)\Big)$$

where R_E is the radius of the Earth, J_{nm} are the harmonic coefficients, F_{nmp}, G_{npq} are the inclination and eccentricity functions, cs_{nm} is the cosine (sine) function if $n-m$ is even (odd) and

$$\Psi_{nmpq}(M,\omega,\Omega,\theta) = (n-2p)\omega + (n-2p+q)M + m(\Omega-\theta) - m\lambda_{nm}\ .$$

- The disturbing functions due to the Sun and Moon have the form (Kaula 1962, Lane 1989):

$$\mathcal{H}_{Sun/Moon/SRP} = \sum \mathcal{A}^{Sun/Moon/SRP}_{k_1k_2k_3k_4k_5k_6}(a,e,i,a_b,e_b,i_b)\cos(k_1M+k_2M_b+k_3\omega+k_4\omega_b+k_5\Omega+$$

respectively, with k_j integers and $b = Sun$ or $Moon$.

Dissipative effects: the atmospheric drag

• The effects of due to the atmospheric drag on the orbital elements are described by averaged equations of the form (see Liu and Alford (1980), Chao (2005))

$$\dot{a} = \frac{1}{2\pi}\int_0^{2\pi} B\,\rho\,\mathcal{F}^{(a)}(a,e,i,M)\,dM\,, \quad \dot{e} = \frac{1}{2\pi}\int_0^{2\pi} B\,\rho\,\mathcal{F}^{(e)}(a,e,i,M)\,dM\,, \quad \frac{di}{dt} = 0,$$

where B is the ballistic coefficient, $\rho(h)$ the atmospheric density as a function of the altitude.

Dissipative effects: the atmospheric drag

• The effects of due to the atmospheric drag on the orbital elements are described by averaged equations of the form (see Liu and Alford (1980), Chao (2005))

$$\dot{a} = \frac{1}{2\pi}\int_0^{2\pi} B\,\rho\,\mathcal{F}^{(a)}(a,e,i,M)\,dM\,, \quad \dot{e} = \frac{1}{2\pi}\int_0^{2\pi} B\,\rho\,\mathcal{F}^{(e)}(a,e,i,M)\,dM\,, \quad \frac{di}{dt} = 0,$$

where B is the ballistic coefficient, $\rho(h)$ the atmospheric density as a function of the altitude.

•The ballistic coefficient can vary by a factor of 10, depending on the satellite's orientation. For instance: LDEF (shape: 12 faces, mass: 9695 kg) $B_{min} = 59\,cm^2/kg$, $B_{max} = 107\,cm^2/kg$; HST (shape: cylinder, mass: 11110 kg) $B_{min} = 50\,cm^2/kg$, $B_{max} = 330\,cm^2/kg$; Explorer 17 (shape: sphere, mass: 188 kg) $B = 65\,cm^2/kg$.

• ISO 27852 (2010), Space systems–Estimation of orbit lifetime: $B \in [25, 500]\,cm^2/kg$.

• In our investigation, we consider B as a constant and we shall often use large values for the ballistic coefficient, up to $2200\,cm^2/kg$ in order to show that orbital decay, caused by the air drag, can be balanced by resonant effects.

• Density models (Jacchia (1971), Mass Spectrometer Incoherent Scatter (MSIS) model (Hedin (1986, 1991))) provide the atmospheric density. The local density is a function of the altitude of the body, the solar flux, the Earth's magnetic index, etc. Of interest is the variation of the density as effect of the solar activity (11–year cycle).
• For the local density we use the barometric formula:

$$\rho(h) = \rho_0 \ \exp\left(-\frac{h - h_0}{H_0}\right) ,$$

where ρ_0 is the (minimum, mean or maximum) density, estimated for (minimum, mean or maximum) solar activity at the reference altitude h_0, while H_0 is the scaling height at h_0 (see MSIS atmospheric model).

• Density models (Jacchia (1971), Mass Spectrometer Incoherent Scatter (MSIS) model (Hedin (1986, 1991))) provide the atmospheric density. The local density is a function of the altitude of the body, the solar flux, the Earth's magnetic index, etc. Of interest is the variation of the density as effect of the solar activity (11–year cycle).
• For the local density we use the barometric formula:

$$\rho(h) = \rho_0 \ \exp\left(-\frac{h-h_0}{H_0}\right),$$

where ρ_0 is the (minimum, mean or maximum) density, estimated for (minimum, mean or maximum) solar activity at the reference altitude h_0, while H_0 is the scaling height at h_0 (see MSIS atmospheric model).
• Using the derivatives

$$\dot{L} = \frac{\partial L}{\partial a}\dot{a}\,, \quad \dot{G} = \dot{L}\sqrt{1-e^2} + \frac{\partial G}{\partial e}\dot{e}\,, \quad \dot{H} = \dot{G}\cos i - G\sin i\,\frac{di}{dt}\,,$$

we derive the functions F_L, F_G and F_H, characterizing the air drag in the dynamical equations expressed in terms of Delaunay variables.

Effects of J_2

• In order to classify the harmonic terms of the Fourier expansions of $\mathcal{H}_{Earth}$, $\mathcal{H}_{Sun}$ and $\mathcal{H}_{Moon}$, it is important to recall the main effects of J_2. Therefore, by considering (compare with King–Hele 1958, Kaula 1966)

$$\mathcal{H}_{Earth} \simeq \frac{R_E^2 J_2 \mu_E^4}{4} \frac{1}{L^3 G^3} \left(1 - 3\frac{H^2}{G^2}\right),$$

where R_E is the radius of the Earth, we get the Hamiltonian

$$\mathcal{H}_{Kepler+J_2} = -\frac{\mu_E^2}{2L^2} + \frac{R_E^2 J_2 \mu_E^4}{4} \frac{1}{L^3 G^3} \left(1 - 3\frac{H^2}{G^2}\right).$$

• Since $\mathcal{H}_{Kepler+J_2}$ depends only on the actions, L, G and H (or equivalently a, e and i) are constant, while the Delaunay angles M, ω and Ω vary linearly in time with the rates

$$\dot{M} \simeq 6135.7\left(\frac{R_E}{a}\right)^{3/2} - 4.98\left(\frac{R_E}{a}\right)^{7/2}(1-e^2)^{-3/2}(1-3\cos^2 i)\ ^o/day\,,$$

$$\dot{\omega} \simeq 4.98\left(\frac{R_E}{a}\right)^{7/2}(1-e^2)^{-2}(5\cos^2 i - 1)\ ^o/day\,,$$

$$\dot{\Omega} \simeq -9.97\left(\frac{R_E}{a}\right)^{7/2}(1-e^2)^{-2}\cos i\ ^o/day\,.$$

• Since $\mathcal{H}_{Kepler+J_2}$ depends only on the actions, L, G and H (or equivalently a, e and i) are constant, while the Delaunay angles M, ω and Ω vary linearly in time with the rates

$$\dot{M} \simeq 6135.7\left(\frac{R_E}{a}\right)^{3/2} - 4.98\left(\frac{R_E}{a}\right)^{7/2}(1-e^2)^{-3/2}(1-3\cos^2 i)\ ^o/day\,,$$

$$\dot{\omega} \simeq 4.98\left(\frac{R_E}{a}\right)^{7/2}(1-e^2)^{-2}(5\cos^2 i - 1)\ ^o/day\,,$$

$$\dot{\Omega} \simeq -9.97\left(\frac{R_E}{a}\right)^{7/2}(1-e^2)^{-2}\cos i\ ^o/day\,.$$

• Therefore, we may summarize as follows the main effects of J_2: a slow change of the rate of the mean anomaly, a precession of the perigee and a secular regression of the orbital node.

Classification of the arguments in the disturbing functions

- The Fourier expansions of $\mathcal{H}_{Earth}$, $\mathcal{H}_{Sun}$ and $\mathcal{H}_{Moon}$ contain infinite number of terms of the form:

$$\mathcal{A}^{Earth}_{k_1k_2k_3k_4}(a,e,i)\cos(k_1M+k_2\theta+k_3\omega+k_4\Omega),$$

$$\mathcal{A}^{Sun/SRP}_{k_1k_2k_3k_4k_5k_6}(a,e,i,a_S,e_S,i_S)\cos(k_1M+k_2M_S+k_3\omega+k_4\omega_S+k_5\Omega+k_6\Omega_S),$$

$$\mathcal{A}^{Moon}_{k_1k_2k_3k_4k_5k_6}(a,e,i,a_M,e_M,i_M)\cos(k_1M+k_2M_M+k_3\omega+k_4\omega_M+k_5\Omega+k_6\Omega_M),$$

respectively, where k_1, k_2, k_3, k_4, k_5 and k_6 are integers.

Classification of the arguments in the disturbing functions

• The Fourier expansions of $\mathcal{H}_{Earth}$, $\mathcal{H}_{Sun}$ and $\mathcal{H}_{Moon}$ contain infinite number of terms of the form:

$$\mathcal{A}^{Earth}_{k_1k_2k_3k_4}(a,e,i)\cos(k_1M+k_2\theta+k_3\omega+k_4\Omega),$$

$$\mathcal{A}^{Sun/SRP}_{k_1k_2k_3k_4k_5k_6}(a,e,i,a_S,e_S,i_S)\cos(k_1M+k_2M_S+k_3\omega+k_4\omega_S+k_5\Omega+k_6\Omega_S),$$

$$\mathcal{A}^{Moon}_{k_1k_2k_3k_4k_5k_6}(a,e,i,a_M,e_M,i_M)\cos(k_1M+k_2M_M+k_3\omega+k_4\omega_M+k_5\Omega+k_6\Omega_M),$$

respectively, where k_1, k_2, k_3, k_4, k_5 and k_6 are integers.

• The angles involved in the above combinations may be classified as follows:

– fast angles: M and θ (since $\dot{M} > 360^\circ/day$ and $\dot{\theta} = 360^\circ/day$);

– semi–fast angles: M_S and M_M (since $\dot{M}_S \simeq 1^\circ/day$ and $\dot{M}_M \simeq 13.06^\circ/day$);

– slow angles: ω, Ω, ω_M, Ω_M (since $\dot{\omega}$ and $\dot{\Omega}$ may be approximated as described in the above Section, ω_S and Ω_S are constant, and $\dot{\omega}_M \simeq 0.164^\circ/day$ and $\dot{\Omega}_M \simeq -0.053^\circ/day$).

• Therefore, we may adopt the following classification of the terms of the expansions:
– *short periodic terms*: the arguments involve the fast angles (M or θ), and $\dot{\theta}$ and $\dot{M}$ are not commensurable;
– *resonant terms*: the arguments involve the fast angles (M or θ), and there is a commensurability between $\dot{\theta}$ and $\dot{M}$;
– *semi–secular terms*: the cosine arguments are independent of the fast angles θ and M, but depend on either M_S or M_M;
– *secular terms*: the cosine arguments are independent of the sidereal time θ and the mean anomalies M, M_S and M_M.

• Therefore, we may adopt the following classification of the terms of the expansions:
– *short periodic terms*: the arguments involve the fast angles (M or θ), and $\dot{\theta}$ and $\dot{M}$ are not commensurable;
– *resonant terms*: the arguments involve the fast angles (M or θ), and there is a commensurability between $\dot{\theta}$ and $\dot{M}$;
– *semi–secular terms*: the cosine arguments are independent of the fast angles θ and M, but depend on either M_S or M_M;
– *secular terms*: the cosine arguments are independent of the sidereal time θ and the mean anomalies M, M_S and M_M.
• There are possible two types of resonances:
i) *tesseral/gravitational resonances*, whenever the period of debris and the rotation of the Earth are commensurable, i.e. $\ell\dot{M} - j\dot{\theta} = 0$, $\ell, j \in \mathbb{N}$, is satisfied. As effect of tesseral resonances, the semi–major axis varies on a time scale of the order of hundred of days.
ii) *lunisolar resonances*, involving a third–body (Sun-Moon) perturber:
- *semi–secular resonances:* involve the mean anomaly of the Sun or of the Moon. These resonances mostly take place in the LEO region.
- *secular resonances:* $k_1\dot{\omega} + k_2\dot{\Omega} + k_3\dot{\omega}_b + k_4\dot{\Omega}_b = 0$, $(k_1, k_2, k_3, k_4) \in \mathbb{Z}^4$, $b = S, M$. Secular resonances provoke long-term variations of eccentricity and inclination on time scales of the order of tens (or hundreds) of years.
- *mean motion resonances:* do not occur in LEO, MEO and GEO.

Outline

1. Introduction
1.1 Origin of space debris
1.2 Breakup events
1.3 The circumterrestrial space
1.4 The LEO environment
1.5 Space debris mitigation strategies

2. Formulation of the problem
2.1 Equations of motion in Cartesian coordinates
2.2 Hamiltonian approach
2.3 Effects of J_2

3. Tesseral resonances
3.1 Tesseral resonances in GEO and MEO
3.2 Tesseral resonances in the LEO region

4. Lunisolar resonances
4.1 Semi–secular resonances
4.2 Secular resonances

5. Conclusions and perspectives

Tesseral resonances in GEO and MEO

• *A tesseral/gravitational resonance* occurs whenever the period of debris and the rotation of the Earth are commensurable, i.e. $\ell\dot{M} - j\dot{\theta} = 0$, $\ell, j \in \mathbb{N}$ is satisfied.

• By using the Kepler's third law, we can estimate the location of tesseral resonances. In fact, we have studied the following resonances:

▷ **In GEO and outside the geostationary ring**: 1:1 resonance at 42164 km from the Earth's center, 2:3 at 55251 km, 1:2 at 66931 km and 1:3 at 87705 km.

▷ **In MEO**: all resonances $j : \ell$, with $j \in \{2, 3, 4, 5\}$, $\ell \in \{1, 2, 3, 4, \}$ and $j > \ell$, namely a total of 9 resonances.

Tesseral resonances in GEO and MEO

• *A tesseral/gravitational resonance* occurs whenever the period of debris and the rotation of the Earth are commensurable, i.e. $\ell\dot{M} - j\dot{\theta} = 0$, $\ell, j \in \mathbb{N}$ is satisfied.
• By using the Kepler's third law, we can estimate the location of tesseral resonances. In fact, we have studied the following resonances:
▷ **In GEO and outside the geostationary ring**: 1:1 resonance at 42164 km from the Earth's center, 2:3 at 55251 km, 1:2 at 66931 km and 1:3 at 87705 km.
▷ **In MEO**: all resonances $j : \ell$, with $j \in \{2, 3, 4, 5\}$, $\ell \in \{1, 2, 3, 4, \}$ and $j > \ell$, namely a total of 9 resonances.
• For each resonance, we approximate $\mathcal{H}_{Earth}$ as: $\mathcal{H}_{Earth} \cong \mathcal{H}^{sec}_{Earth} + \mathcal{H}^{res\, j:\ell}_{Earth}$, and provide explicit expressions for $\mathcal{H}^{sec}_{Earth}$, $\mathcal{H}^{res\, j:\ell}_{Earth}$, which can be handled analytically.
• Analyzing the dominant terms, namely the terms prevailing in specific regions of the parameter space, we reduce the Hamiltonian to a toy model similar to a pendulum.
• The toy model provides: location of equilibria, amplitude of libration regions, occurrence of splitting or overlapping of the resonant islands, bifurcations.
• These results are confirmed by numerical studies based on the Cartesian equations and by computing the FLIs.

• We consider the Earth's gravitational potential up to terms of degree and order $n = m = 4$. Averaging over the fast angles, we approximate $\mathcal{H}_{Earth}$ by

$$\mathcal{H}_{Earth} \approx \mathcal{H}^{sec}_{Earth} + \mathcal{H}^{res}_{Earth} \ ,$$

where $\mathcal{H}^{sec}_{earth}$, $\mathcal{H}^{res}_{earth}$ are the secular and resonant parts.

• We consider the Earth's gravitational potential up to terms of degree and order $n = m = 4$. Averaging over the fast angles, we approximate $\mathcal{H}_{Earth}$ by

$$\mathcal{H}_{Earth} \approx \mathcal{H}^{sec}_{Earth} + \mathcal{H}^{res}_{Earth} \ ,$$

where $\mathcal{H}^{sec}_{earth}$, $\mathcal{H}^{res}_{earth}$ are the secular and resonant parts.

• Up to second order in eccentricity, the secular part is given by:

$$\begin{aligned}
\mathcal{H}^{sec}_{Earth} \cong & \frac{\mu_E R_E^2 J_2}{a^3}\left(\frac{3}{4}\sin^2 i - \frac{1}{2}\right)(1-e^2)^{-3/2} \\
& + \frac{2\mu_E R_E^3 J_3}{a^4}\left(\frac{15}{16}\sin^3 i - \frac{3}{4}\sin i\right)e(1-e^2)^{-5/2}\sin\omega \\
& + \frac{\mu_E R_E^4 J_4}{a^5}\left[\left(-\frac{35}{32}\sin^4 i + \frac{15}{16}\sin^2 i\right)\frac{3e^2}{2}(1-e^2)^{-7/2}\cos(2\omega)\right. \\
& \left. + \left(\frac{105}{64}\sin^4 i - \frac{15}{8}\sin^2 i + \frac{3}{8}\right)(1+\frac{3e^2}{2})(1-e^2)^{-7/2}\right].
\end{aligned} \tag{2}$$

The 1:1 resonance

- We denote by λ the so called "stroboscopic mean node":

$$\lambda = M + \omega + \Omega - \theta.$$

- Up to second order in e and taking $n = m = 4$, we consider 20 terms of the expansion of the 1:1 resonant part:

$$\begin{aligned}
\mathcal{H}^{res1:1}_{Earth} &\simeq \frac{\mu_E R_E^2 J_{22}}{a^3}\left\{\frac{3}{4}(1+\cos i)^2\left(1-\frac{5}{2}e^2\right)\cos[2(\lambda-\lambda_{22})]\right\} \\
&+ \frac{\mu_E R_E^3 J_{31}}{a^4}\left\{\left(\frac{15}{16}\sin^2 i(1+3\cos i)-\frac{3}{4}(1+\cos i)\right)(1+2e^2)\cos(\lambda-\lambda_{31})\right\} \\
&+ \frac{\mu_E R_E^2 J_{22}}{a^3}\left\{\frac{27}{8}e^2\sin^2 i\cos[2(\lambda-\omega-\lambda_{22})]\right\}+\ldots \\
&\cong t_1+t_2+t_3+\ldots
\end{aligned}$$

The 1:1 resonance

- We denote by λ the so called "stroboscopic mean node":

$$\lambda = M + \omega + \Omega - \theta.$$

- Up to second order in e and taking $n = m = 4$, we consider 20 terms of the expansion of the 1:1 resonant part:

$$\begin{aligned}
\mathcal{H}^{res1:1}_{Earth} &\simeq \frac{\mu_E R_E^2 J_{22}}{a^3}\left\{\frac{3}{4}(1+\cos i)^2\left(1-\frac{5}{2}e^2\right)\cos[2(\lambda-\lambda_{22})]\right\} \\
&+ \frac{\mu_E R_E^3 J_{31}}{a^4}\left\{\left(\frac{15}{16}\sin^2 i(1+3\cos i)-\frac{3}{4}(1+\cos i)\right)(1+2e^2)\cos(\lambda-\lambda_{31})\right\} \\
&+ \frac{\mu_E R_E^2 J_{22}}{a^3}\left\{\frac{27}{8}e^2\sin^2 i\cos[2(\lambda-\omega-\lambda_{22})]\right\}+\ldots \\
&\cong t_1+t_2+t_3+\ldots
\end{aligned}$$

Definition. A specific term, for example $f_1(L,G,H)\cos[2(\lambda-\lambda_{22})]$ of the expansion of $R^{res1:1}_{Earth}$, is dominant in a given region of phase space, if $|f_1(L,G,H)|$ is greater than the magnitude of any other term of the expansion in that region.

$$\mathcal{H}_{Earth} \simeq \mathcal{H}^{sec}_{Earth} + \frac{\mu_E R_E^2 J_{22}}{a^3}\left\{\frac{3}{4}(1+\cos i)^2(1-\frac{5}{2}e^2)\cos[2(\lambda-\lambda_{22})]\right\} + t_2 + t_3 \ldots$$

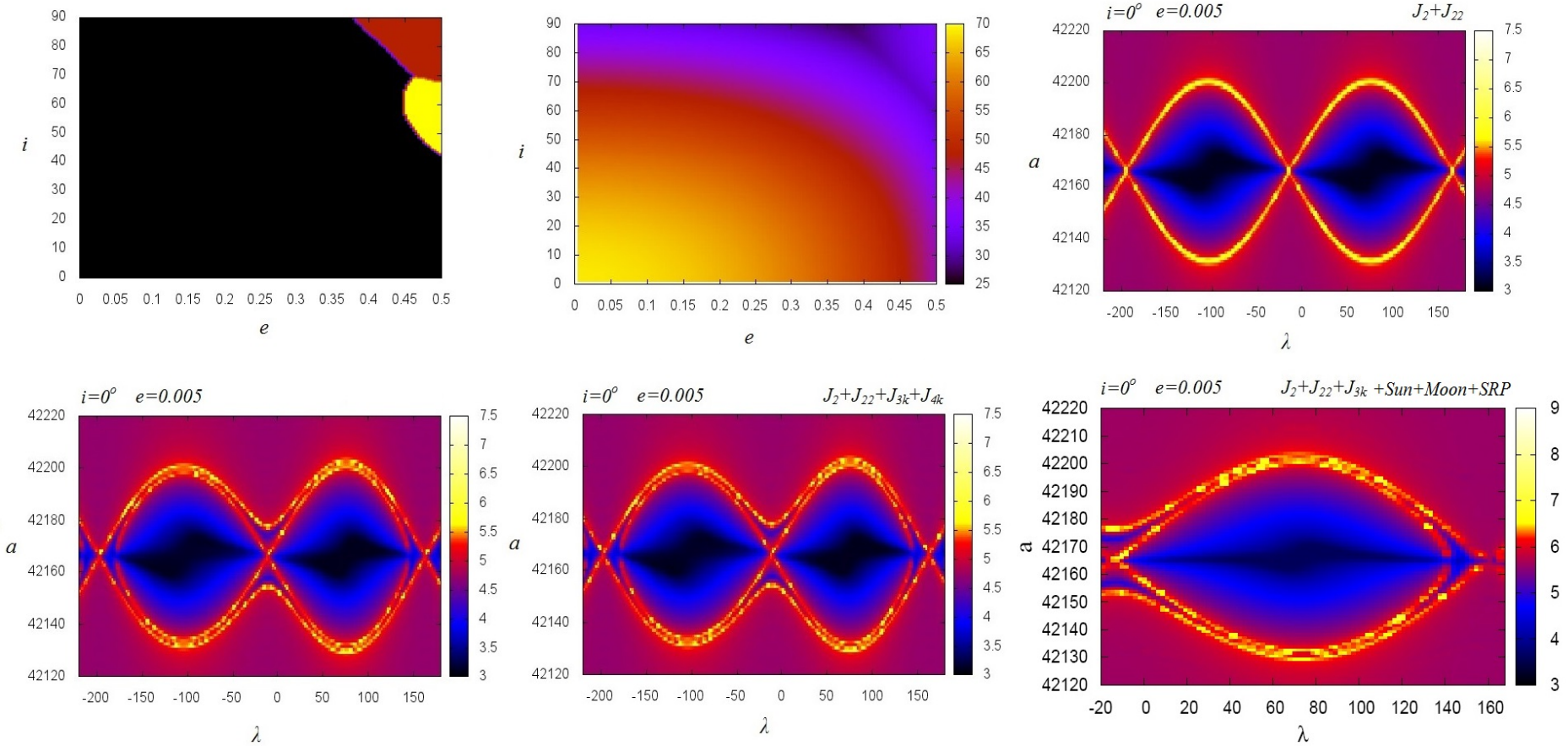

Figure : Top left: Dominant term for $a = a_{res}$; Top middle: Amplitude of resonance; Top right and bottom: FLI for $i = 0^o$, $e = 0.005$, $\Omega = 0^o$ and $\omega = 0^o$.

The 2:1 resonance

$$\mathcal{H}^{res2:1}_{Earth} \simeq t_1 + t_2 + t_3 \ldots \qquad \sigma_{21} = M - 2\theta + \omega + 2\Omega$$

$$t_1 = \frac{\mu_E R_E^2 J_{22}}{a^3}\left\{\frac{3}{4}(1+\cos i)^2\left(-\frac{e}{2}\right)\cos(\sigma_{21}+\omega-2\lambda_{22})\right\},$$

$$t_2 = \frac{\mu_E R_E^2 J_{22}}{a^3}\left\{\frac{3}{2}\sin^2 i\left(\frac{3}{2}e\right)\cos(\sigma_{21}-\omega-2\lambda_{22})\right\}$$

$$t_3 = \frac{\mu_E R_E^3 J_{32}}{a^4}\left\{\frac{15}{8}\sin i(1-2\cos i-3\cos^2 i)\left(1+2e^2\right)\sin(\sigma_{21}-2\lambda_{32})\right\}\ldots$$

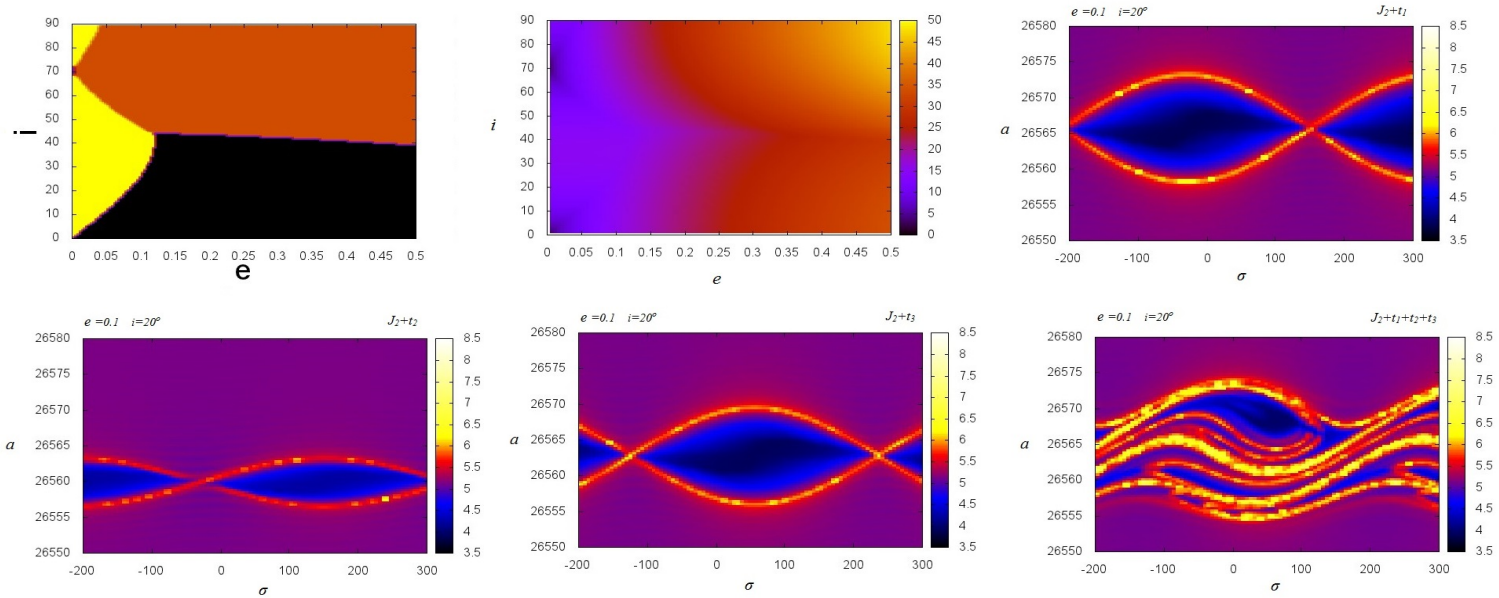

Figure : Top left: Dominant term for $a = a_{res}$; Top middle: Amplitude of resonance; Top right and bottom: FLI for $i = 20^o$, $e = 0.1$, $\Omega = 0^o$ and $\omega = 0^o$.

Transcritical bifurcations (2:1 resonance)

• Each of the following terms dominates in some region of the phase space. As a consequence, the widths and the location of the resonant island's centers depend on e and i. Chaotic motions are possible when two terms are comparable in magnitude;

$$
\begin{aligned}
t_1 &= \frac{\mu_E R_E^2 J_{22}}{a^3}\left\{\frac{3}{4}(1+\cos i)^2\left(-\frac{e}{2}\right)\right\}\cos(\sigma_{21}+\omega-2\lambda_{22}) \\
t_2 &= \frac{\mu_E R_E^2 J_{22}}{a^3}\left\{\frac{3}{2}\sin^2 i\left(\frac{3}{2}e\right)\right\}\cos(\sigma_{21}-\omega-2\lambda_{22}) \\
t_3 &= \frac{\mu_E R_E^3 J_{32}}{a^4}\left\{\frac{15}{8}\sin i(1-2\cos i-3\cos^2 i)\left(1+2e^2\right)\right\}\sin(\sigma_{21}-2\lambda_{32}),
\end{aligned}
\tag{3}
$$

• t_3 is dominant for small e; the function

$$
f:[0^o,90^o]\longrightarrow\mathbb{R},\qquad f(i)=-\sin i(1-2\cos i-3\cos^2 i), \tag{4}
$$

changes sign at 70.53^o.

• At $i = 70.53^o$ the stability of equilibria reverses. For $i < 70.53^o$ the stable point is at about $\sigma_{21} \simeq 55^o$ and the unstable at $\sigma_{21} \simeq 235^o$, while for $i > 70.53^o$ the situation is opposite: the hyperbolic point is at $\sigma \simeq 55^o$ and the stable at $\sigma \simeq 235^o$.
Conclusion: at $i = 70.53^o$ we have a transcritical bifurcation point.

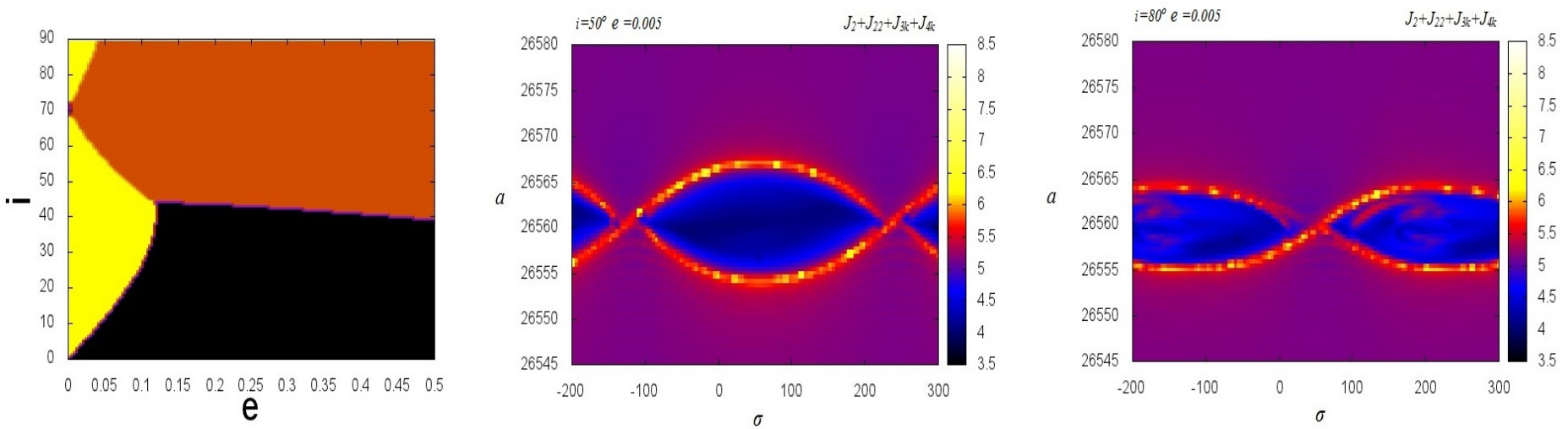

Figure : The transcritical bifurcation phenomenon. FLI for the MEO 2:1 resonance, for $e = 0.005$, $\omega = 0$, $\Omega = 0$: $i = 50$ (left); $i = 80$ (right).

Splitting and overlapping of resonances. The 5:1 resonance

- $\mathcal{H}^{res5:1}_{Earth} \simeq \sum_{q\in\mathbb{Z}} \mathcal{A}_q(L,G,H)\cos[\sigma_{51}+q\omega+const.]\,,\quad \sigma_{51}=M-5\theta+\omega+5\Omega.$
- We recall that the secular part, in particular J_2 (see for example Kaula 1966), provokes a precession of perigee, that is $\dot{\omega}\simeq \frac{3}{2}nJ_2(\frac{R_E}{a(1-e^2)})^2(2-\frac{5}{2}\sin^2 i)$.
- If $i\neq 63.4^o$ then $\dot{\omega}\neq 0$ and the angles $\sigma_{51}+q\omega$, $\omega\in\mathbb{Z}$, have zero derivatives at different locations. So, the resonance splits into a multiplet of resonances.
- From $\dot{\sigma}_{51}+q\dot{\omega}=0, q\in\mathbb{Z}$ we get the location of each libration island of the multiplet. Moreover, we can compute the amplitude of each libration island.
- So, when the sum of the sizes of the amplitudes of two islands is smaller than the distance between the resonances then we have the splitting phenomenon (regular motions). Otherwise, we get the overlap of resonances and the onset of chaos.

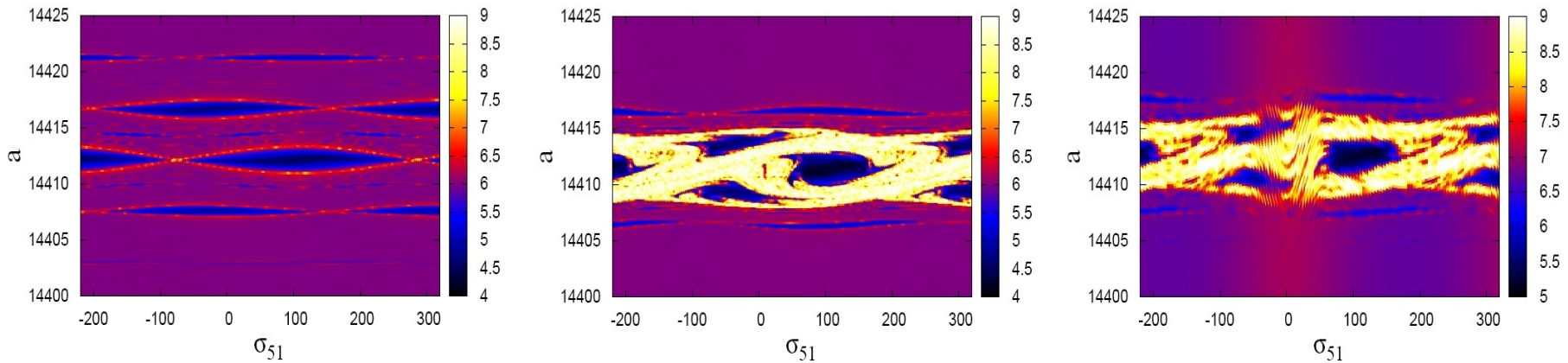

Figure : Left: $i=30^o$, $e=0.2$, Middle and right: $i=45^o$, $e=0.2$. Left and middle: Hamiltonian equations; Right: Cartesian equations, including Sun, Moon and SRP.

Tesseral resonances in the LEO region

- *A tesseral/gravitational resonance* occurs whenever the period of debris and the rotation of the Earth are commensurable, i.e. $(n - 2p + q)\dot{M} - m\dot{\theta} \cong 0$ is satisfied.
- We study the resonances $11:1$, $12:1$, $13:1$ and $14:1$. We focus on the orbits for which $e \in [0, 0.2]$ and $i \in [0^o, 120^o]$.
- By using the Kepler's third law, the altitude of these resonances is estimated at:

$m:1$	a (km)	Altitude (km)	Perigee altitude for $e = 0.02$ (km)	Apogee altitude for $e = 0.02$ (km)
11:1	8524.75	2146.61	1976.25	2317.25
12:1	8044.32	1666.18	1505.43	1827.21
13:1	7626.31	1248.17	1095.78	1400.84
14:1	7258.69	880.55	735.52	1025.86

Tesseral resonances in the LEO region

- *A tesseral/gravitational resonance* occurs whenever the period of debris and the rotation of the Earth are commensurable, i.e. $(n - 2p + q)\dot{M} - m\dot{\theta} \cong 0$ is satisfied.
- We study the resonances $11:1$, $12:1$, $13:1$ and $14:1$. We focus on the orbits for which $e \in [0, 0.2]$ and $i \in [0^o, 120^o]$.
- By using the Kepler's third law, the altitude of these resonances is estimated at:

$m:1$	a (km)	Altitude (km)	Perigee altitude for $e = 0.02$ (km)	Apogee altitude for $e = 0.02$ (km)
11:1	8524.75	2146.61	1976.25	2317.25
12:1	8044.32	1666.18	1505.43	1827.21
13:1	7626.31	1248.17	1095.78	1400.84
14:1	7258.69	880.55	735.52	1025.86

- For each resonance, we approximate $\mathcal{H}_{Earth}$ as: $\mathcal{H}_{Earth} \cong \mathcal{H}^{sec}_{Earth} + \mathcal{H}^{res\, m:1}_{Earth}$.
- The analysis of the dominant terms shows that 5 of the resonant part are relevant. In a more compact notation, $\mathcal{H}^{res\, m:1}_{earth}$ is written as:

$$\mathcal{H}^{res\, m:1}_{earth} = \mathcal{A}^{(m)}_0(L, G, H)\cos(\sigma_{m1} - \varphi^{(m)}_0), \quad \text{with} \quad \sigma_{m1} = M - m\theta + \omega + m\Omega.$$

• Our study is based on the following models:
◇ Model 1 (or the toy model): a 1 d.o.f. problem which considers the effects of: the Keplerian part, a J_2 approximation for the secular part, the resonant part contains just on the dominant terms (5 terms), while the dissipative part is characterized by the function $F_{_L}$ and the effect of the solar cycle is disregarded. The toy model is described by the following equations:

$$\dot{\sigma}_{m1} = h^{(m)}_{,L}(L,G,H) + \varepsilon \mathcal{A}^{(m)}_{,L}(L,G,H)\ \cos(\sigma_{m1} - \varphi^{(m)})\ ,$$

$$\dot{L} = \varepsilon \mathcal{A}^{(m)}(L,G,H)\sin(\sigma_{m1} - \varphi^{(m)}) - \eta D^{(m)}_{_L}(L,G,H)\ ,$$

where the actions G and H are considered constants, ε is a small parameter (of the order of 10^{-9}), artificially introduced so that the functions $h^{(m)}$, $\mathcal{A}^{(m)}$ and $D^{(m)}_{_L}$ have comparable magnitudes, and $\eta = B\rho$ is the dissipation parameter.
◇ Model 2 (or the dissipative model of LEO resonances (DMLR)): a 3 d.o.f. problem described in terms of the Keplerian part, the disturbing function due to the Earth $\mathcal{H}_{Earth}$ and the dissipative functions $F_{_L}$, $F_{_G}$, $F_{_H}$. The effect of the solar cycle is disregarded.
◇ Model 3 (or the full model): all effects, including the solar cycle, and the influence of the Moon and Sun.

Amplitude of resonances

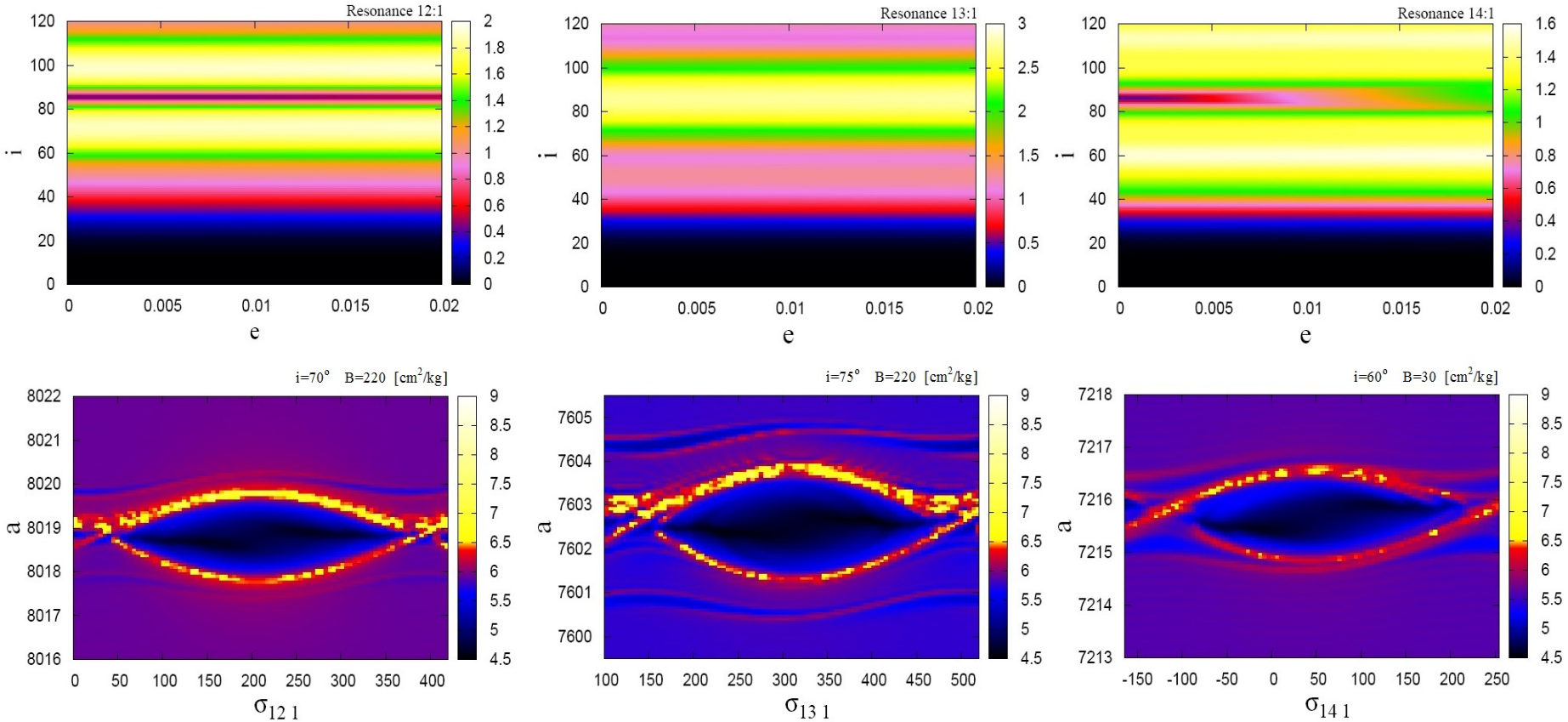

Figure : Top: The amplitude of resonances computed by using the conservative toy model (model 1). Bottom: FLI (using DMLR or the model 2) for $e = 0.005$, $\Omega = 0^o$, $\omega = 0^o$ and mean atmospheric density.

Existence of equilibrium points

Theorem

For fixed values of $e \in [0, 0.02]$ *and* $i \in [0^o, 120^o]$ *(or equivalently, given* G_0 *and* H_0 *in the corresponding intervals), let* $(\sigma_{m1}^{(0)}, L_0)$ *be an equilibrium point for the conservative toy model. Assume that* η, ε *satisfy the inequalities:*

$$\left| \frac{\eta D_L^{(m)}(L_0, G_0, H_0)}{\varepsilon \mathcal{A}^{(m)}(L_0, G_0, H_0)} \right| \leq 1 - \delta \,, \qquad \gamma_1 \varepsilon + \gamma_2 \eta + \gamma_3 \varepsilon^2 < \delta,$$

for some positive constants δ, γ_1, γ_2 *and* γ_3. *Then, the dissipative toy model admits equilibrium points. At first order in* η, *the point* $(\sigma_{m1}^{(1)}, L_1)$ *defined by*

$$\sigma_{m1}^{(1)} = \sigma_{m1}^{(0)} + \frac{D_L^{(m)}(L_0, G_0, H_0)}{\varepsilon \mathcal{A}^{(m)}(L_0, G_0, H_0) \cos(\sigma_{m1}^0 - \varphi^{(m)})} \eta \,, \qquad L_1 = L_0$$

is an equilibrium point for the dissipative model.

- Stability: if $(\sigma_{m1}^{(0)}, L_0)$ is a center (saddle) for the conservative toy model, then $(\sigma_{m1}^{(1)}, L_1)$ is an unstable spiral (saddle) for the dissipative toy model.

Position of equilibrium points

- Dissipative toy model: locate immediately the position of equilibria.

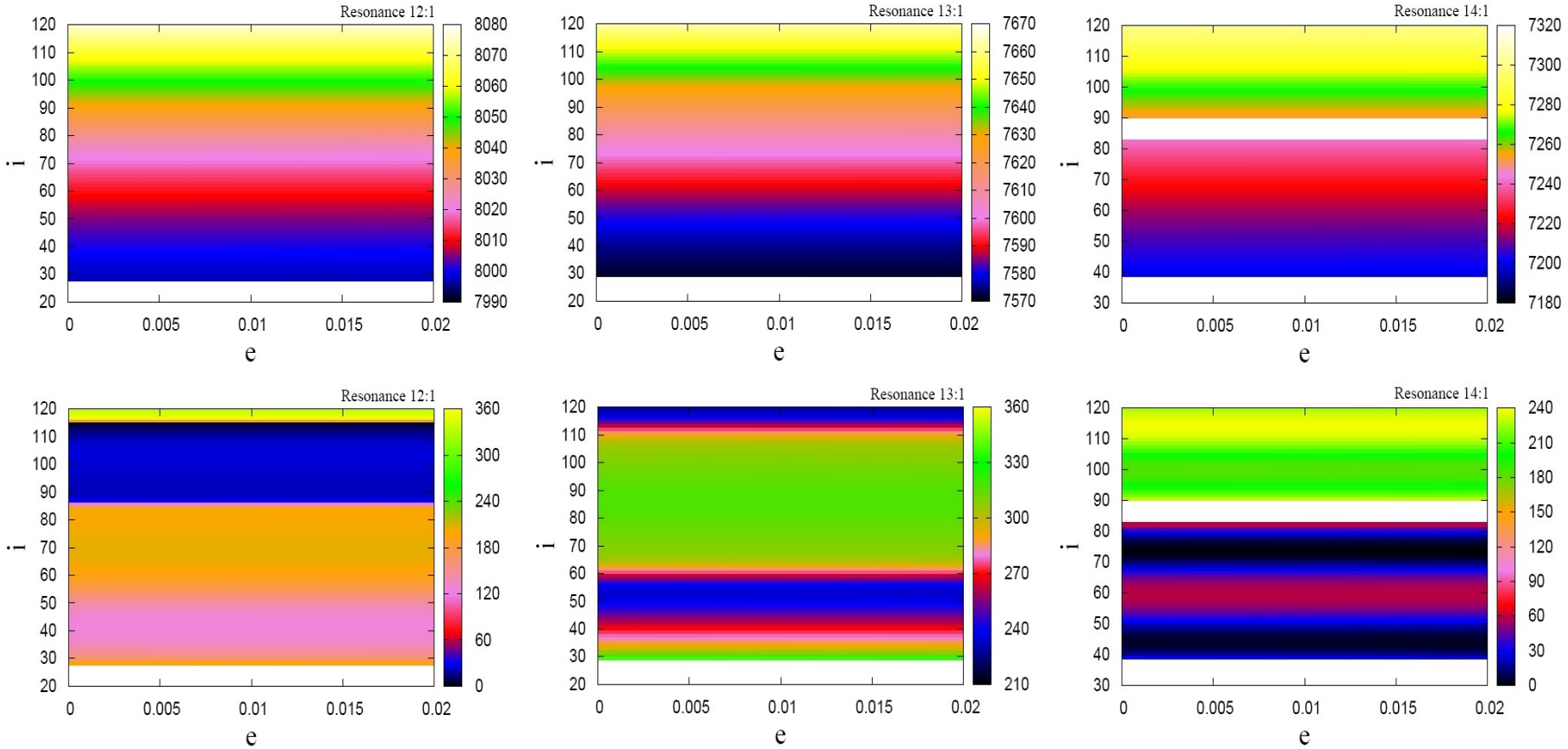

Figure : Position of equilibrium points as a function of eccentricity and inclination, for $B = 220\,[cm^2/kg]$ and mean atmospheric density. Top: semimajor axis; Bottom: resonant angle.

Shift of equilibria along the σ_{m1} axis

- Existence theorem: varying the value of η, the equilibria shift along the σ_{m1} axis.

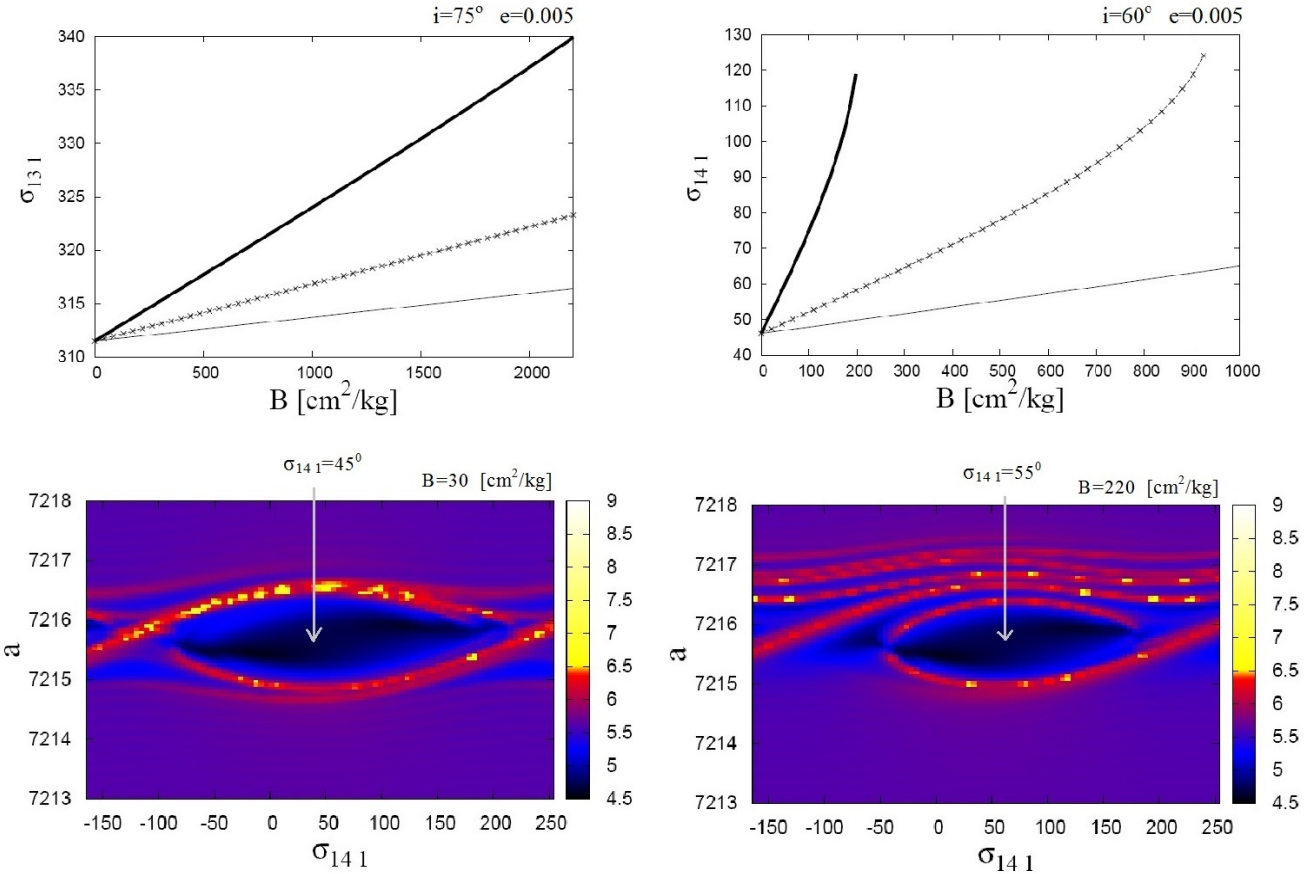

Figure : Top: Location of spiral points (using DMLR) on the σ_{m1} axis, as a function of B, for the minimum (thinner line), medium (dotted line) and maximum (thicker line) values of the atmospheric density. Bottom: FLI (using DMLR) for mean atmospheric density and for $B = 30\,[cm^2/kg]$ (left) and $B = 220\,[cm^2/kg]$ (right)

A quantitative study of resonances

- Numerical evidence that the above results hold under a more complete model.
- Use of the full model (model 3): Earth+Sun+Moon+solar cycle.
- Usually the long-term evolution of the semi-major axis is little influenced by the lunisolar perturbations. However, there are some cases showing a remarkable difference. An orbit reaching the resonant region, either it passes through resonance or it is temporary captured into resonance. This behavior has a strongly stochastic feature. A small perturbation, or a small change in the initial conditions, leads to a different scenario.

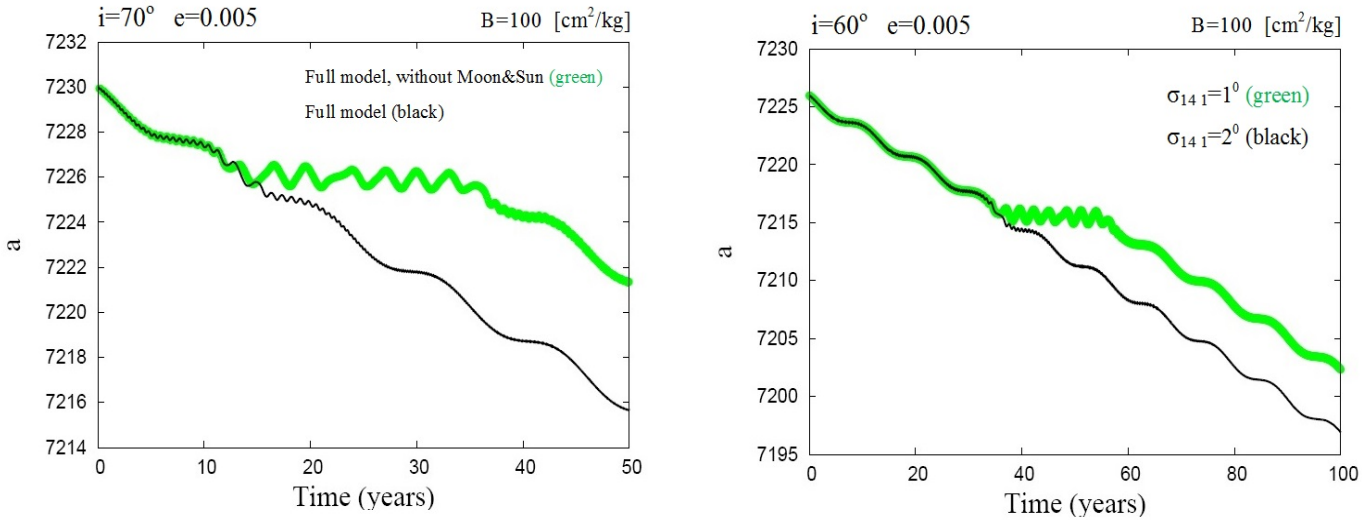

Figure : The 14:1 resonance (using the full model): temporary capture into resonance (green) and passage through the resonance (black).

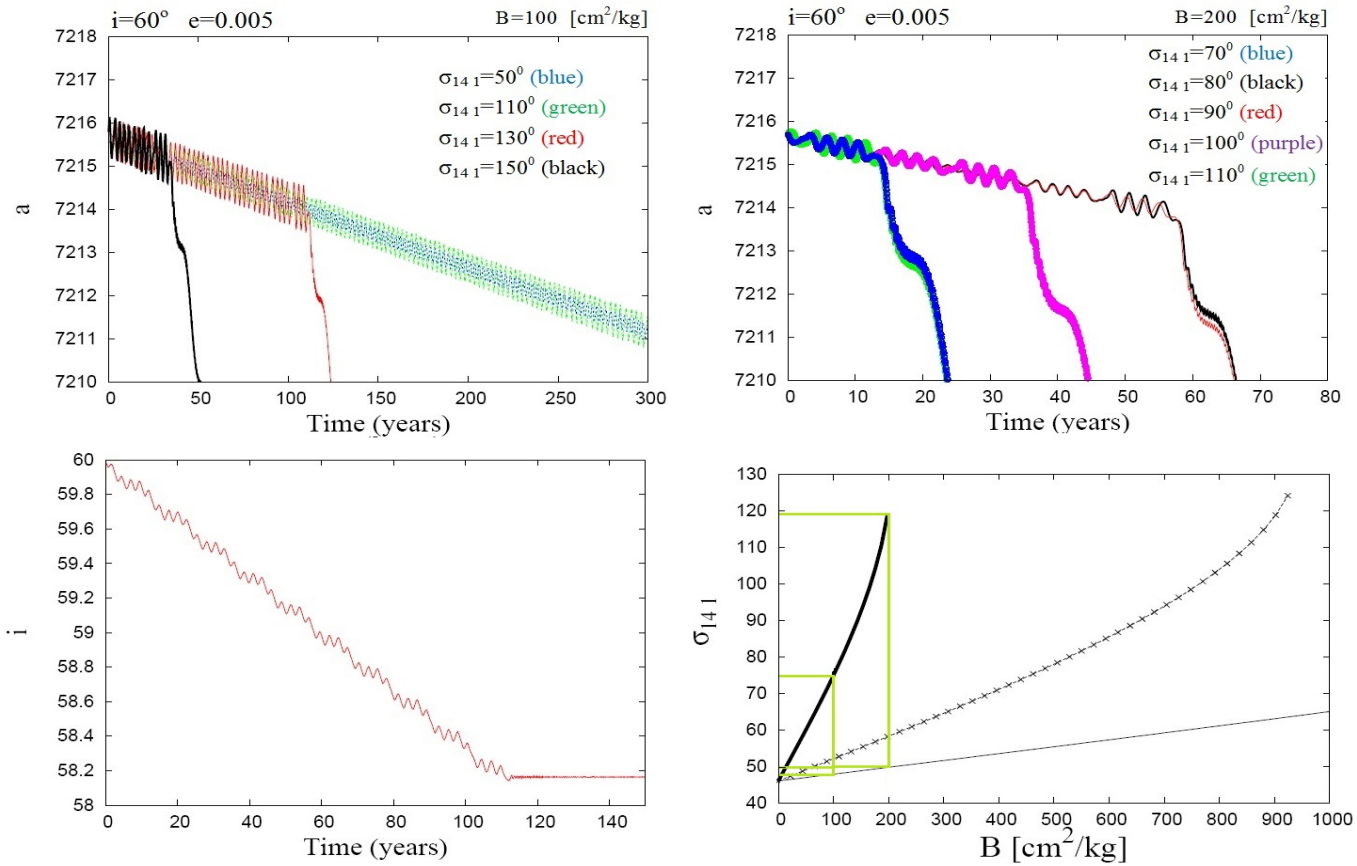

Figure : Behavior of the semi–major axis inside the 14:1 resonance: trapped motions (top left: blue and green) and escape motions (top left: red and black and top right). These phenomena are described better when they are corroborated with the results shown in the bottom left plot, which shows that for $B = 100\ [cm^2/kg]$, the position of the spiral point oscillates between 47^o and 75^o, while for $B = 200\ [cm^2/kg]$, between 50^o and 120^o.

Outline

1. Introduction
1.1 Origin of space debris
1.2 Breakup events
1.3 The circumterrestrial space
1.4 The LEO environment
1.5 Space debris mitigation strategies

2. Formulation of the problem
2.1 Equations of motion in Cartesian coordinates
2.2 Hamiltonian approach
2.3 Effects of J_2

3. Tesseral resonances
3.1 Tesseral resonances in GEO and MEO
3.2 Tesseral resonances in the LEO region

4. Lunisolar resonances
4.1 Semi–secular resonances
4.2 Secular resonances

5. Conclusions and perspectives

Semi–secular resonances

- Solar semi-secular resonances are characterized by a relation of the form

$$\alpha\dot{\omega} + \beta\dot{\Omega} - \gamma\dot{M}_S = 0 \ ,$$

where (within the quadrupolar approximation) $\alpha = 0, \pm 2$, $\beta = 0, \pm 1, \pm 2$, $\gamma \neq 0$. We can set $\dot{M}_S = 1\ ^o$/day. Lunar semi–secular resonances can be defined in a similar way.

- Fixing the semimajor axis and eccentricity, it is easy to determine the inclination so that the above equation is satisfied.

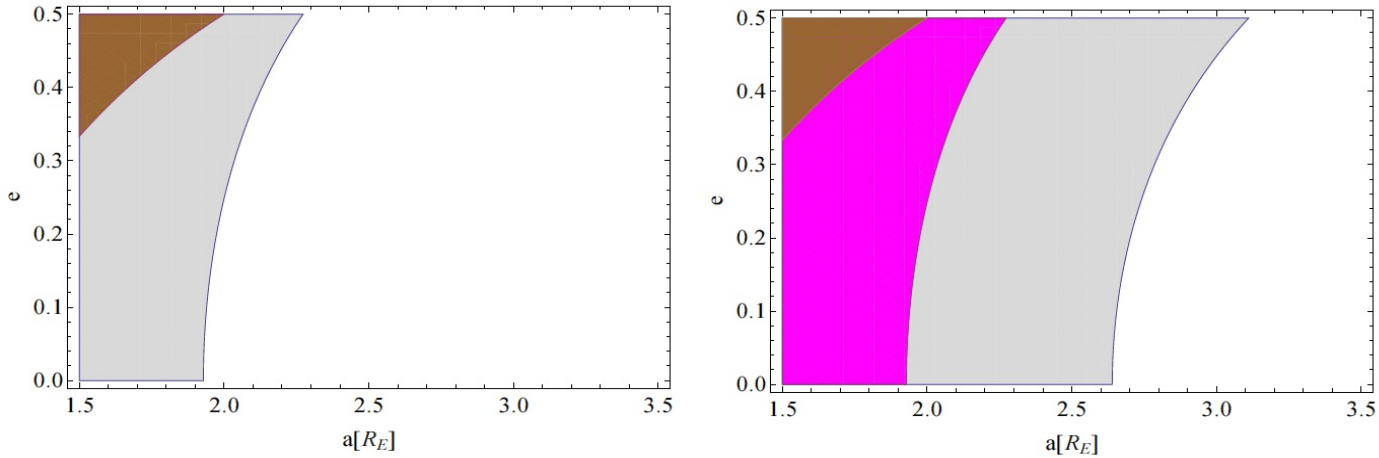

Figure : The regions in the (a, e) plane, where the above equation admits solutions. Semi-secular resonances with $\alpha = 0$, $\beta = 2$, $\gamma = 2$ (left) and $\alpha = 2$, $\beta = 2$, $\gamma = 2$ (right). Legend: white – no solutions, light grey – one solution, purple – two solutions, brown–colliding orbits.

• For $e \leq 0.5$, the semi–secular resonances occur in LEO and in vicinity of the LEO region, thus ω and Ω, as well as M_S, M_M and M are fast angles in comparison with the resonant angle $\sigma = \alpha\omega + \beta\Omega - \gamma M_S$.

• The dynamics of a specific semi-secular resonance can be described by a reduced model, which is obtained by averaging the full Hamiltonian over M, M_S, M_M, ω and Ω, and retaining only the secular and resonant terms.

• From a dynamical perspective the semi-secular resonances can be grouped in two classes: resonances with $\alpha = 0$ and resonances with $\alpha \neq 0$, respectively. The effect of the resonances from the class $\alpha = 0$ is a variation of the inclination.
• Let us consider a resonance for which $\alpha \neq 0$. The model can be reduced to the one degree-of-freedom Hamiltonian:

$$\mathcal{K}_{\alpha\beta\gamma}(\Lambda, \sigma; \Gamma, L) = f_0(\Lambda; \Gamma, L) - \gamma \dot{M}_S \Lambda + f_1(\Lambda; \Gamma, L) \cos(\sigma - \sigma_0)\,,$$

where

$$\Lambda = \frac{1}{\alpha} G\,, \qquad \Gamma = H - \frac{\beta}{\alpha} G\,.$$

L and Λ are constants.

- The equilibria are obtained by solving the equations

$$\frac{\partial f_0}{\partial \Lambda} - \gamma \dot{M}_S + \frac{\partial f_1}{\partial \Lambda} \cos(\sigma - \sigma_0) = 0, \qquad f_1 \sin(\sigma - \sigma_0) = 0\,.$$

- Solving the above equations for Λ and σ we distinguish the cases:

Case (a): if there exist L_0 and Γ_0 so that $f_1(\Lambda; \Gamma_0, L_0) = 0$ admits solutions, let Λ_0 be one of them (for instance, for the resonance with $\alpha = \beta = \gamma = 2$ the function f_1 vanishes either for $e = 0$ or $i = 180^0$).

One has either $(a)_1$: $\frac{\partial f_1}{\partial \Lambda}(\Lambda_0; \Gamma_0, L_0) = 0$ and $\frac{\partial f_0}{\partial \Lambda}(\Lambda_0; \Gamma_0, L_0) - \gamma \dot{M}_S = 0$;

or $(a)_2$: $\frac{\partial f_1}{\partial \Lambda}(\Lambda_0; \Gamma_0, L_0) \neq 0$ and $\left|\frac{\partial f_0}{\partial \Lambda}(\Lambda_0; \Gamma_0, L_0) - \gamma \dot{M}_S\right| \leq \left|\frac{\partial f_1}{\partial \Lambda}(\Lambda_0; \Gamma_0, L_0)\right|$.

Case (b): if $\sigma = \sigma_0 + 180^o k$, where $k \in \mathbb{Z}$, then the second equation is identically satisfied. Substituting σ in the first equation of we deduce the values of Λ corresponding to equilibria, provided these exist.

$(b)_1$ we can solve the first equations both when $\sigma = \sigma_0 + 360^o k$ and $\sigma = \sigma_0 + 180^o + 360^o k$;

or $(b)_2$ we can solve the first equations just when $\sigma = \sigma_0 + 360^o k$ or $\sigma = \sigma_0 + 180^o + 360^o k$;

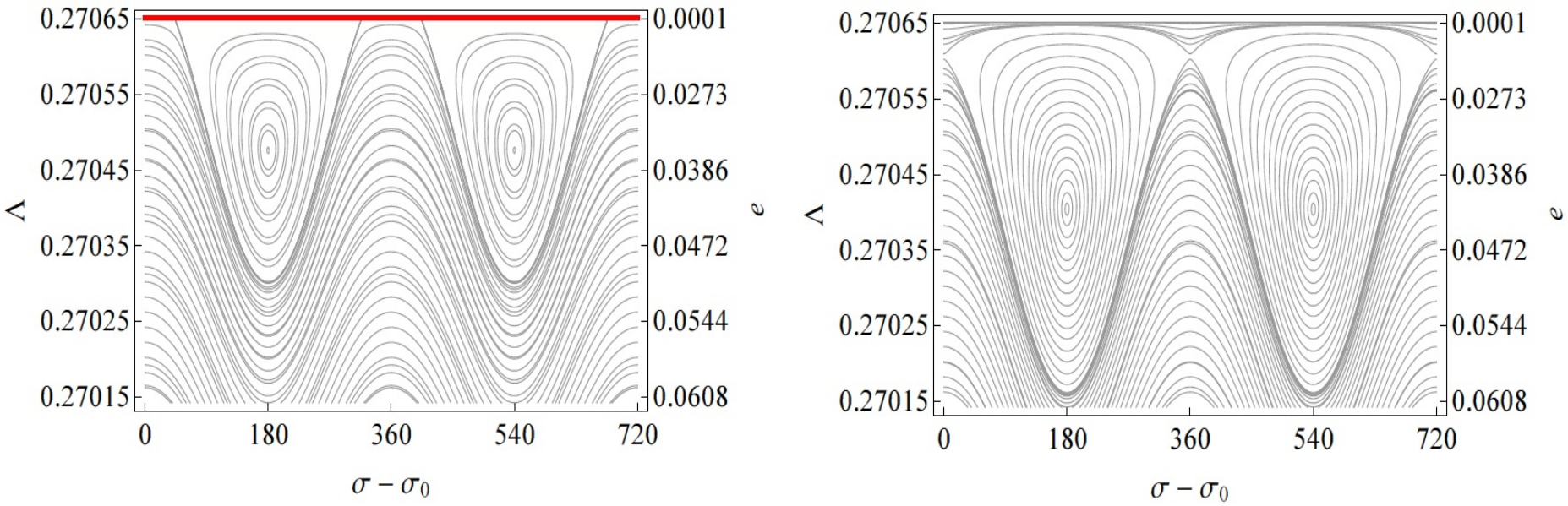

Figure : Phase portrait of the resonance $\alpha = \beta = \gamma = 2$ in the $(\sigma - \sigma_0, \Lambda)$-plane, showing a bifurcation of equilibria: stable equilibrium points at $\sigma - \sigma_0 = 180^o + 360^o k$, $k \in \mathbb{Z}$ (left plots), and respectively stable and unstable equilibria at $\sigma - \sigma_0 = 180^o k$, $k \in \mathbb{Z}$ (right plot). The plots are obtained for some fixed values of L and Γ which was obtained by giving a, e and i. For the left plot L and Γ correspond to $a = 1.937 R_E$, $e = 0.1$, $i = 1.51^o$, while the right plot is obtained for $a = 1.937 R_E$, $e = 0.1$, $i = 2.01^o$. On the left plot, all points on the horizontal line $e = 0$ (red line) are equilibrium points, that is the conditions of the case $(a)_1$ are satisfied.

Secular resonances

• Let us suppose that the region of interest is outside the libration regions of tesseral resonances. Then, in MEO, one may reduce the problem to the following Hamiltonian:

$$\mathcal{H}^{sec} = \mathcal{H}^{sec}_{Earth} + \mathcal{H}^{sec}_{Sun} + \mathcal{H}^{sec}_{Moon} ,$$

where

$$\mathcal{H}^{sec}_{Earth} = \frac{R_E^2 J_2 \mu_E^4}{4} \frac{1}{L^3 G^3} \left(1 - 3\frac{H^2}{G^2}\right),$$

namely we consider only the most important contribution, corresponding to the J_2 gravity coefficient of the Earth's perturbation.
Moreover, $\mathcal{H}^{sec}_{Sun}$ and $\mathcal{H}^{sec}_{Moon}$ are defined by averaging $\mathcal{H}_{Sun}$ and $\mathcal{H}_{Moon}$ over both the mean anomaly M and the mean anomaly M_b of the perturbing body, as well as by truncating the series expansions up to the second order in the ratio a/a_b, with $b = S, M$ (quadrupolar approximation).

Secular resonances

• Let us suppose that the region of interest is outside the libration regions of tesseral resonances. Then, in MEO, one may reduce the problem to the following Hamiltonian:

$$\mathcal{H}^{sec} = \mathcal{H}^{sec}_{Earth} + \mathcal{H}^{sec}_{Sun} + \mathcal{H}^{sec}_{Moon},$$

where

$$\mathcal{H}^{sec}_{Earth} = \frac{R_E^2 J_2 \mu_E^4}{4} \frac{1}{L^3 G^3} \left(1 - 3\frac{H^2}{G^2}\right),$$

namely we consider only the most important contribution, corresponding to the J_2 gravity coefficient of the Earth's perturbation.
Moreover, $\mathcal{H}^{sec}_{Sun}$ and $\mathcal{H}^{sec}_{Moon}$ are defined by averaging $\mathcal{H}_{Sun}$ and $\mathcal{H}_{Moon}$ over both the mean anomaly M and the mean anomaly M_b of the perturbing body, as well as by truncating the series expansions up to the second order in the ratio a/a_b, with $b = S, M$ (quadrupolar approximation).
• We neglected the Keplerian part, since M is an ignorable variable, and so, L is constant.
• $\mathcal{H}^{sec}$ depends on time only through Ω_M, which varies linearly with the rate $\dot{\Omega}_M \simeq -0.053^\circ/day$.
In conclusion, the Hamiltonian $\mathcal{H}^{sec}$ is *a two degrees of freedom non-autonomous Hamiltonian*, depending on the parameter L.

Validation of the Hamiltonian model

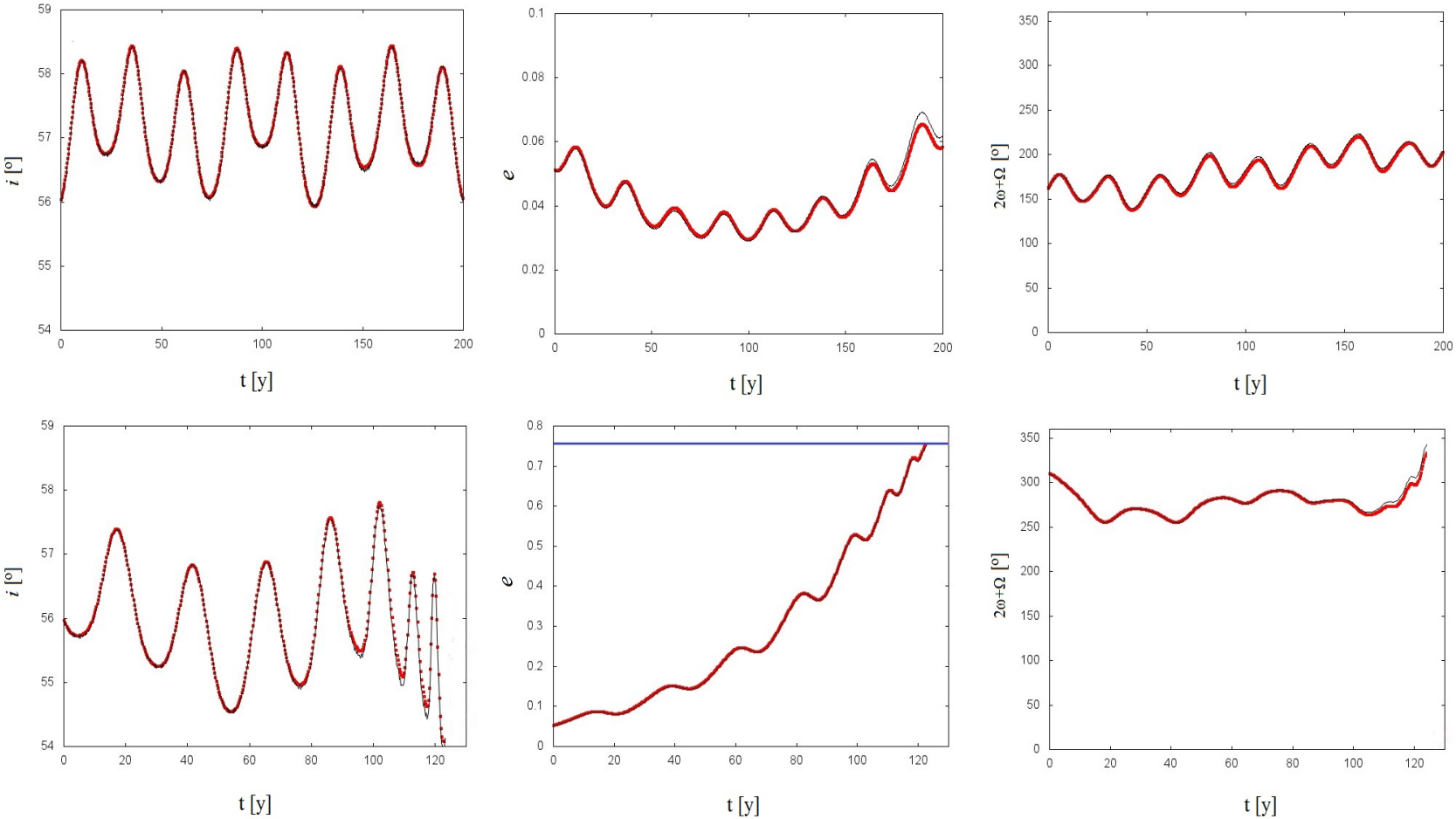

Figure : Integration of the two orbits for which $a = 26\,520\,km$, $e(0) = 0.05122$, $i(0) = 56^o$, and $\omega(0) = 190^o$, $\Omega(0) = 140^o$ (top panels), respectively, $\omega(0) = 30^o$, $\Omega(0) = 250^o$ (bottom plots). Red color – Hamiltonian formulation, black color – Cartesian model. Blue line – the eccentricity value leading to re-entry.

Types of secular resonances

- The secular parts $\mathcal{H}^{sec}_{Sun}$ and $\mathcal{H}^{sec}_{Moon}$ have the form (Kaula 1962, Lane 1989, Daquin et al. 2015, Celletti et al. 2016)

$$\mathcal{H}^{sec}_{Sun} = \sum_{m=0}^{2} \sum_{p=0}^{2} \mathcal{A}^{Sun}_{mp}(a, a_S, e, e_S, i, i_S) \cos\Big((2-2p)\omega + m(\Omega - \Omega_S) \Big) \ ,$$

and

$$\mathcal{H}^{sec}_{Moon} = \sum_{m=0}^{2} \sum_{s=0}^{2} \sum_{p=0}^{2} \mathcal{A}^{Moon}_{msp}(a, a_M, e, e_M, i, i_M) \cos\Big((2-2p)\omega + m\Omega \pm s\Omega_M \Big) \ .$$

• In MEO, there are possible two types of secular resonances:
i)the ones that do not involve the rate $\dot{\Omega}_M$, namely

$$(2-2p)\dot{\omega}+m\dot{\Omega}=0\,,$$

called also as resonances depending only on inclination
ii) and the resonances

$$(2-2p)\dot{\omega}+m\dot{\Omega}+\kappa\dot{\Omega}_M=0, \qquad \kappa\neq 0.$$

• In MEO, there are possible two types of secular resonances:
i)the ones that do not involve the rate $\dot{\Omega}_M$, namely

$$(2-2p)\dot{\omega}+m\dot{\Omega}=0\,,$$

called also as resonances depending only on inclination
ii) and the resonances

$$(2-2p)\dot{\omega}+m\dot{\Omega}+\kappa\dot{\Omega}_M=0, \qquad \kappa\neq 0.$$

• The name of *resonances depending on inclination* is justified if one takes into account the relations:

$$\dot{\omega}\simeq 4.98\left(\frac{R_E}{a}\right)^{7/2}(1-e^2)^{-2}(5\cos^2 i-1)\ ^o/day\,,$$

$$\dot{\Omega}\simeq -9.97\left(\frac{R_E}{a}\right)^{7/2}(1-e^2)^{-2}\cos i\ ^o/day\,.$$

Combining linearly $\dot{\omega}$ and $\dot{\Omega}$ we obtain a relation depending only on the inclination.

- The resonances depending on inclination are located as follows:

$$\dot{\omega} = 0 \qquad \text{at} \quad 63.4^\circ \quad \text{or} \quad 116.4^\circ \,,$$

$$\dot{\Omega} = 0 \qquad \text{at} \quad 90^\circ \,,$$

$$\dot{\omega} + \dot{\Omega} = 0 \qquad \text{at} \quad 46.4^\circ \quad \text{or} \quad 106.9^\circ \,,$$

$$-\dot{\omega} + \dot{\Omega} = 0 \qquad \text{at} \quad 73.2^\circ \quad \text{or} \quad 133.6^\circ \,,$$

$$-2\dot{\omega} + \dot{\Omega} = 0 \qquad \text{at} \quad 69.0^\circ \quad \text{or} \quad 123.9^\circ \,,$$

$$2\dot{\omega} + \dot{\Omega} = 0 \qquad \text{at} \quad 56.1^\circ \quad \text{or} \quad 111.0^\circ \,.$$

• The resonances depending on inclination are located as follows:

$$\dot{\omega} = 0 \qquad at \quad 63.4^\circ \quad or \quad 116.4^\circ \,,$$

$$\dot{\Omega} = 0 \qquad at \quad 90^\circ \,,$$

$$\dot{\omega} + \dot{\Omega} = 0 \qquad at \quad 46.4^\circ \quad or \quad 106.9^\circ \,,$$

$$-\dot{\omega} + \dot{\Omega} = 0 \qquad at \quad 73.2^\circ \quad or \quad 133.6^\circ \,,$$

$$-2\dot{\omega} + \dot{\Omega} = 0 \qquad at \quad 69.0^\circ \quad or \quad 123.9^\circ \,,$$

$$2\dot{\omega} + \dot{\Omega} = 0 \qquad at \quad 56.1^\circ \quad or \quad 111.0^\circ \,.$$

• The resonances involving the lunar ascending node Ω_M are responsible for the existence of a web–like structure of resonances in the phase space (Ely and Howell 1997, Rosengren 2015, Celletti and Galeş 2016, Daquin 2016).

• The resonances depending on inclination are located as follows:

$$\dot{\omega} = 0 \qquad at \quad 63.4^\circ \quad or \quad 116.4^\circ \,,$$

$$\dot{\Omega} = 0 \qquad at \quad 90^\circ \,,$$

$$\dot{\omega} + \dot{\Omega} = 0 \qquad at \quad 46.4^\circ \quad or \quad 106.9^\circ \,,$$

$$-\dot{\omega} + \dot{\Omega} = 0 \qquad at \quad 73.2^\circ \quad or \quad 133.6^\circ \,,$$

$$-2\dot{\omega} + \dot{\Omega} = 0 \qquad at \quad 69.0^\circ \quad or \quad 123.9^\circ \,,$$

$$2\dot{\omega} + \dot{\Omega} = 0 \qquad at \quad 56.1^\circ \quad or \quad 111.0^\circ \,.$$

• The resonances involving the lunar ascending node Ω_M are responsible for the existence of a web–like structure of resonances in the phase space (Ely and Howell 1997, Rosengren 2015, Celletti and Galeş 2016, Daquin 2016).

• Next plots show the web structure of the resonances in the plane (G, H). The units of length and time are normalized so that the geostationary distance is unity (it amounts to 42 164.1696 km) and that the period of Earth's rotation is equal to 2π.

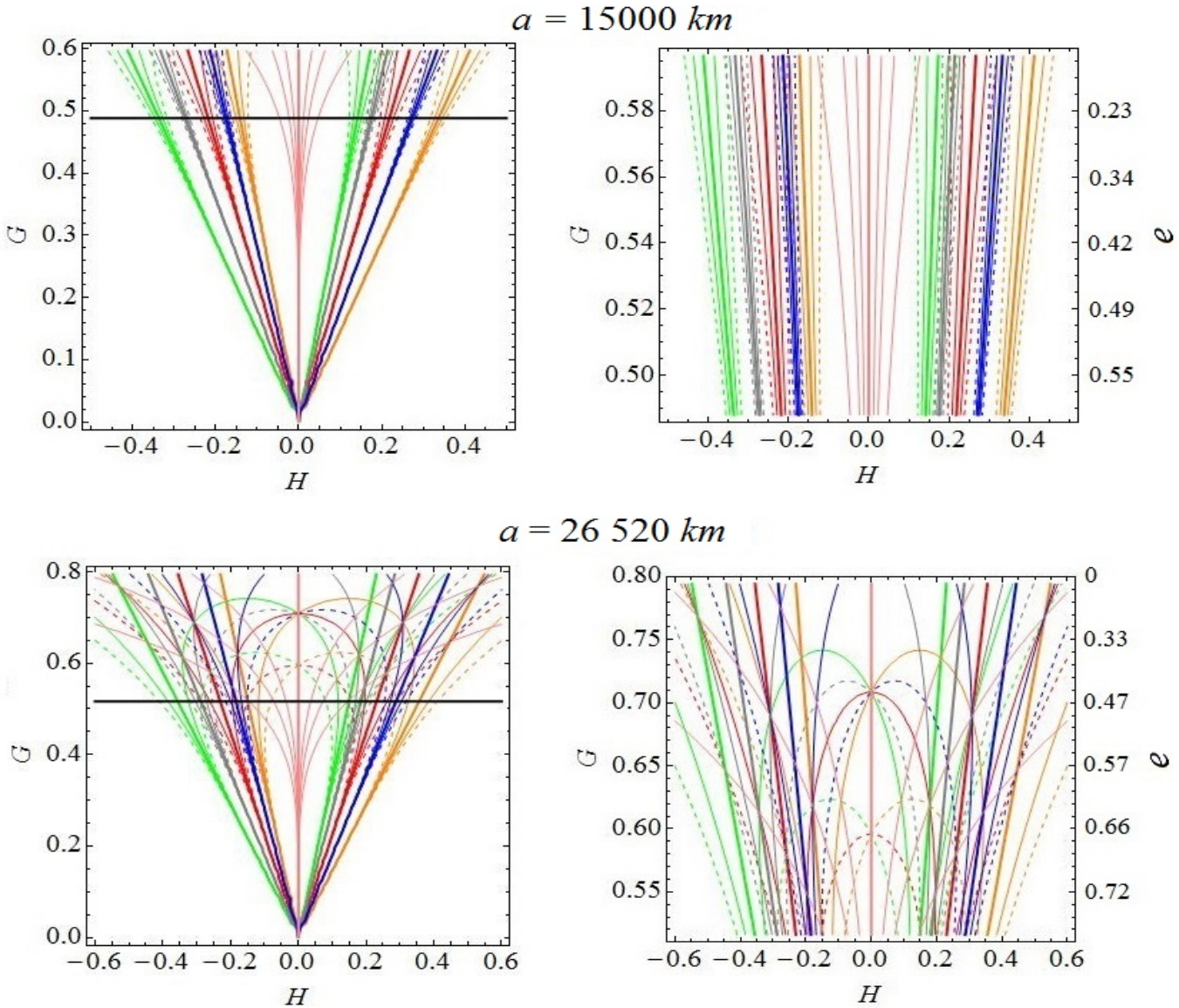

Figure : The web structure of lunisolar resonances: $\dot{\omega} + \dot{\Omega} = 0$ (orange color, $i = 46.4°$, $i = 106.9°$); $2\dot{\omega} + \dot{\Omega} = 0$ (blue color, $i = 56.1°$, $i = 111°$); $\dot{\omega} = 0$ (red color, $i = 63.4°$, $i = 116.6°$); $2\dot{\omega} - \dot{\Omega} = 0$ (grey color, $i = 69.0°$); $\dot{\omega} - \dot{\Omega} = 0$ (green color, $i = 73.2°$, $i = 133.6°$); $\dot{\Omega} = 0$ (pink color, $i = 90°$)

Effects of secular resonances

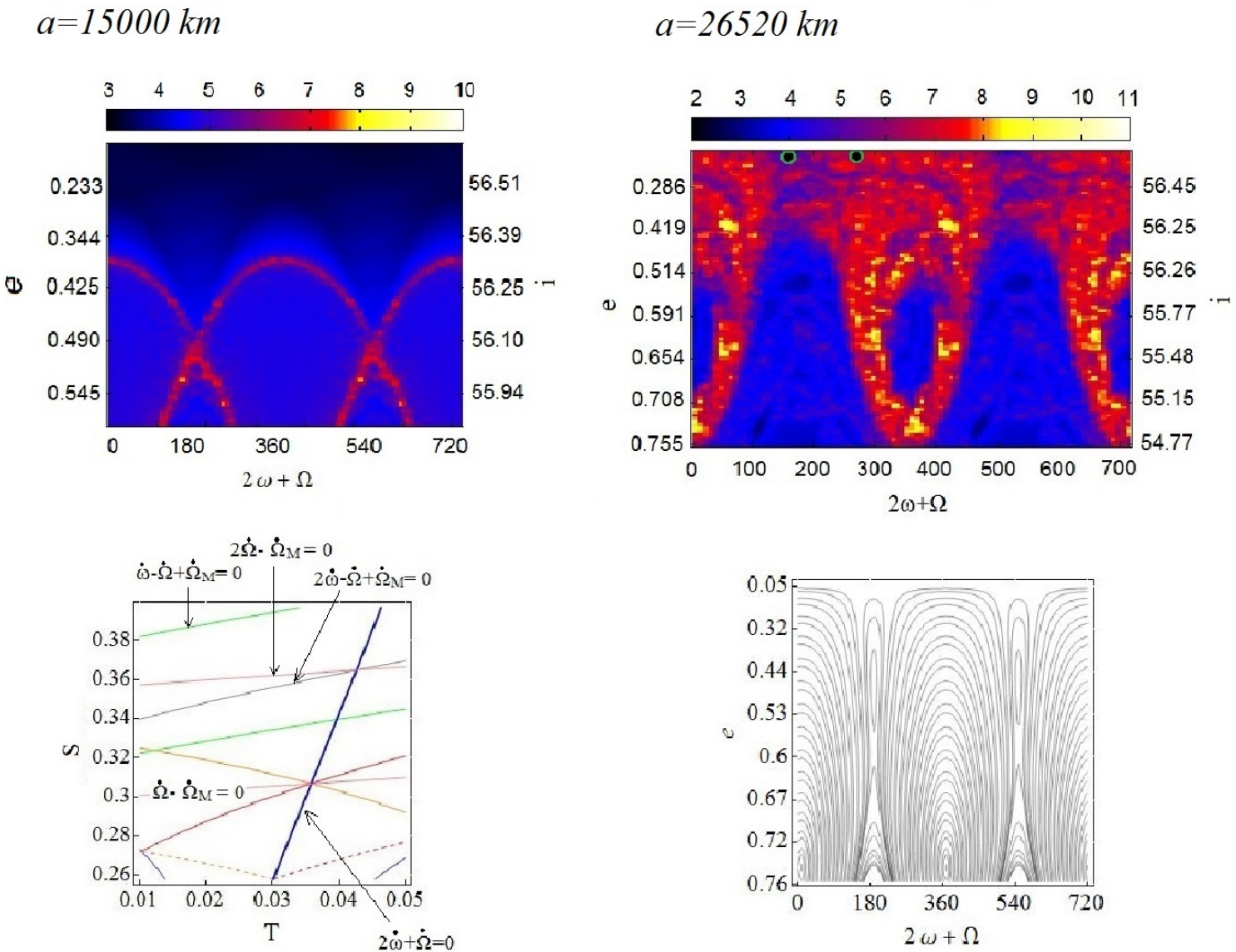

Figure : Top: The FLI for $a = 1500$ km (left) and $a = 26520$ km (right). Bottom ($a = 26520$ km): the web structure of resonances (left) and the phase portrait (right).

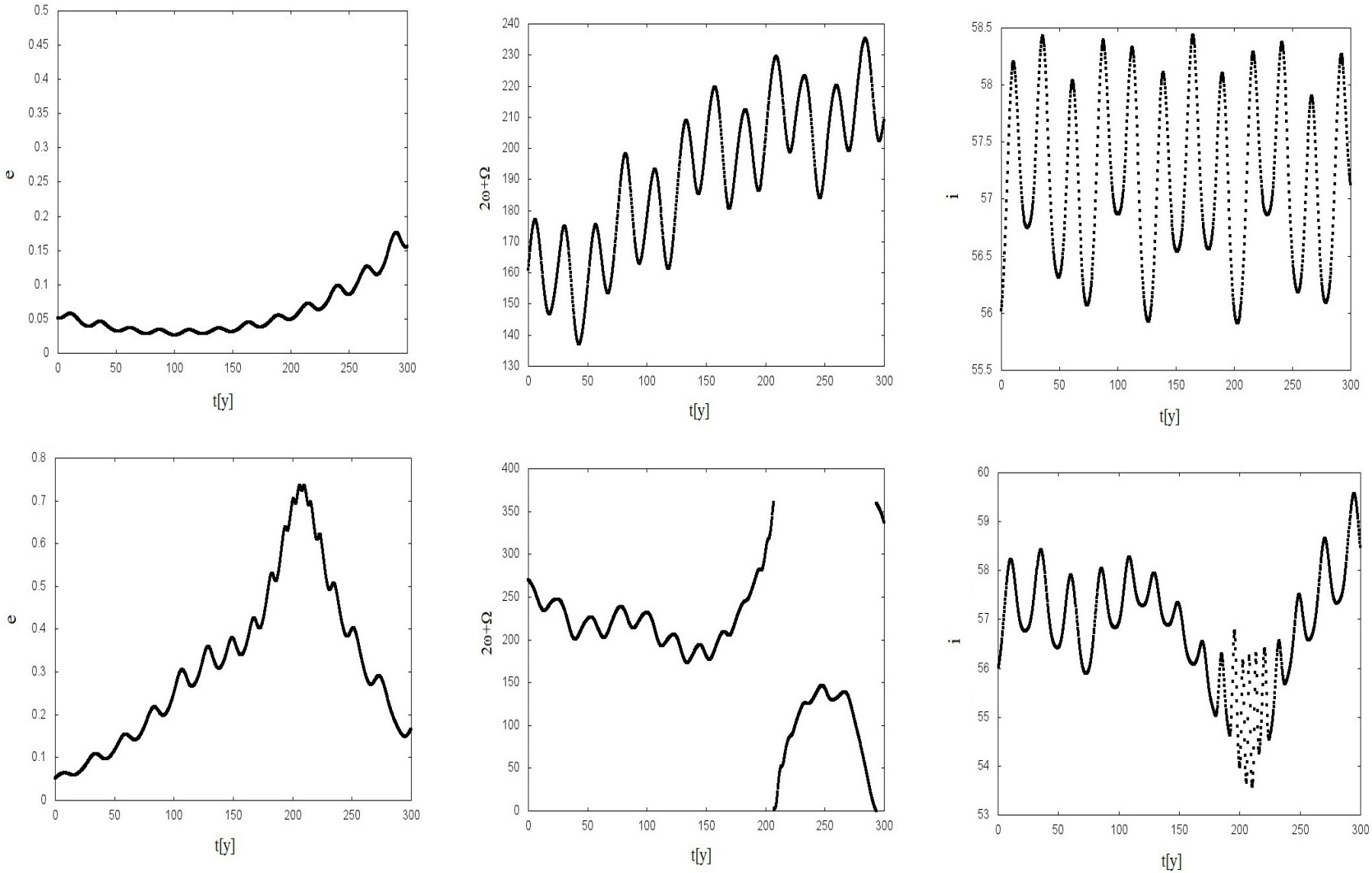

Figure : Integration of the orbits: $a = 26\,520\,km$, $e(0) = 0.05122$, $i(0) = 56^o$, $\Omega(0) = 140^o$ and $\omega(0) = 190^o$ (top) and respectively $\omega(0) = 65^o$ (bottom).

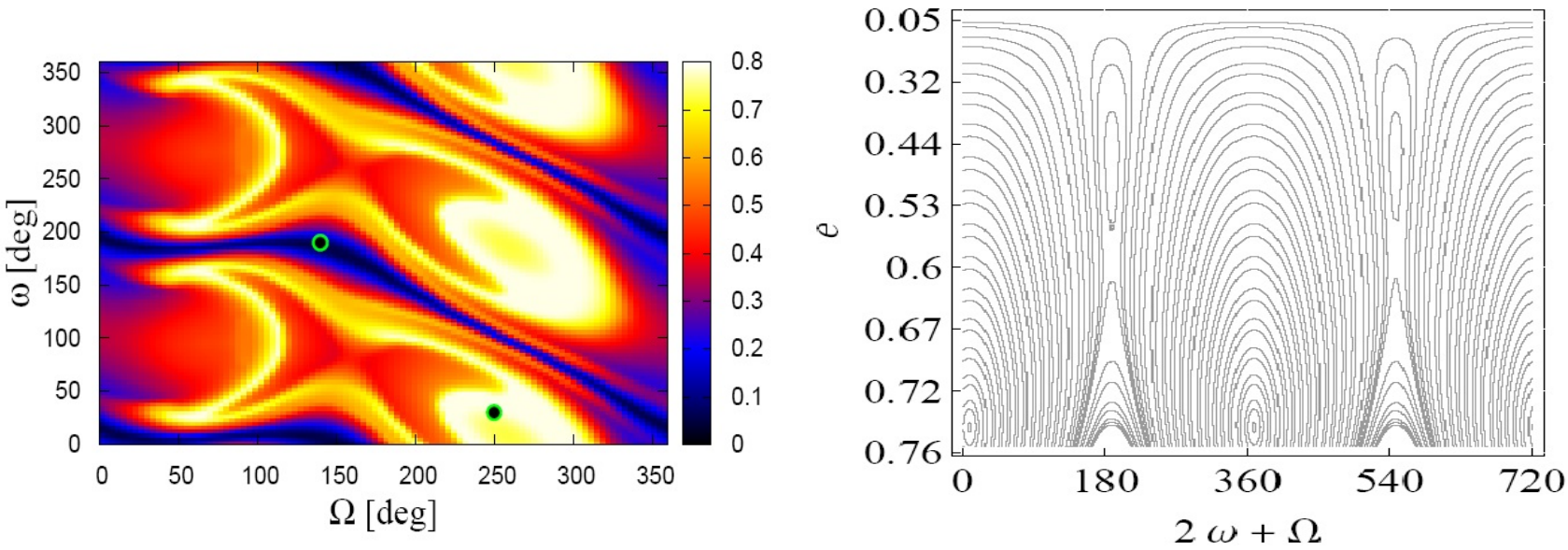

Figure : Left panel: Maximum eccentricity reached in 200 years (color bar) as a function of ω and Ω. The other initial conditions are $a(0) = 26\,520\,km$, $e(0) = 0.05122$ and $i(0) = 56^o$ at the initial Epoch J2000 (Jan. 1, 2000, 12:00 GMT). Right panel: bifurcation of equilibria, as shown by the one–degree–of–freedom model a). The phase space portrait is obtained for the same value $a = 26\,520\,km$ of the semi–major axis as for the left panel.

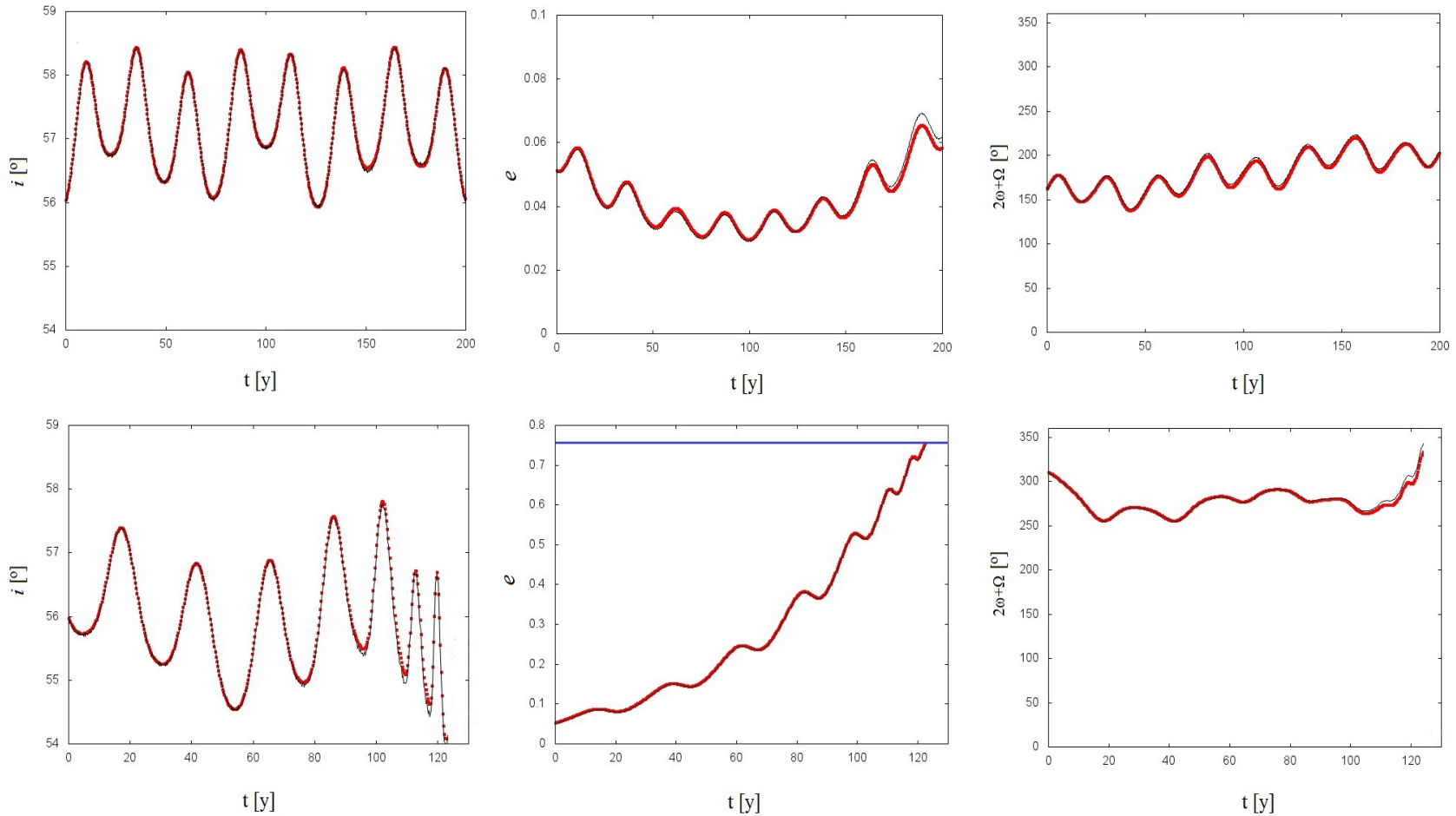

Figure : Integration of the two orbits for which $a = 26\,520\,km$, $e(0) = 0.05122$, $i(0) = 56^o$, and $\omega(0) = 190^o$, $\Omega(0) = 140^o$ (top panels), respectively, $\omega(0) = 30^o$, $\Omega(0) = 250^o$ (bottom plots). Red color – Hamiltonian formulation, black color – Cartesian model. Blue line – the eccentricity value leading to re-entry.

Outline

1. Introduction
1.1 Origin of space debris
1.2 Breakup events
1.3 The circumterrestrial space
1.4 The LEO environment
1.5 Space debris mitigation strategies

2. Formulation of the problem
2.1 Equations of motion in Cartesian coordinates
2.2 Hamiltonian approach
2.3 Effects of J_2

3. Tesseral resonances
3.1 Tesseral resonances in GEO and MEO
3.2 Tesseral resonances in the LEO region

4. Lunisolar resonances
4.1 Semi–secular resonances
4.2 Secular resonances

5. Conclusions and perspectives

Conclusions and perspectives

Conclusions:

- study of tesseral, lunisecular resonances, using numerical and analytical tools;
- tesseral resonances induce variations the semi-major axis, while lunisecular resonances provoke variations of the eccentricity and inclination;
- numerical and analytical study of the LEO tesseral resonances: orbital decay, caused by the air drag, can be balanced by resonant effects, for a large class of values of dynamic parameters (ballistic coefficient, inclination, eccentricity, etc.);
- occurrence of a plethora of dynamical phenomena in LEO: temporary capture into resonance, passage through resonance, trapped motions, escape motions, shift of equilibria along some axes, bifurcations, etc.
- lunisolar secular resonances: bifurcations, overlapping of resonances, chaotic variation of semimajor axis, eccentricity and inclination.

Conclusions and perspectives

Conclusions:

- study of tesseral, lunisecular resonances, using numerical and analytical tools;
- tesseral resonances induce variations the semi-major axis, while lunisecular resonances provoke variations of the eccentricity and inclination;
- numerical and analytical study of the LEO tesseral resonances: orbital decay, caused by the air drag, can be balanced by resonant effects, for a large class of values of dynamic parameters (ballistic coefficient, inclination, eccentricity, etc.);
- occurrence of a plethora of dynamical phenomena in LEO: temporary capture into resonance, passage through resonance, trapped motions, escape motions, shift of equilibria along some axes, bifurcations, etc.
- lunisolar secular resonances: bifurcations, overlapping of resonances, chaotic variation of semimajor axis, eccentricity and inclination.

Perspectives:

- a more detailed analysis of the LEO resonance in order to discriminate between the possibility of parking satellites in the close vicinity of equilibrium points, or, on the contrary, to avoid such zones due to a possible accumulation of a large number of space debris in these regions;
- analyze concrete examples and design suitable disposal orbits;
- simulate breakup events and analyse the evolution of debris clouds;

References

• A. Celletti, C. G., *On the dynamics of space debris: 1:1 and 2:1 resonances*, J. Nonlinear Science 2014.

• A. Celletti, C. G., *Dynamics of minor resonances for space debris*, Cel. Mech. Dyn. Astr. 2015.

• A. Celletti, C. G., *A study of the main resonances outside the geostationary ring*, Advances in Space Research, 2015.

• A. Celletti, C. G., G. Pucacco, *Bifurcation of lunisolar secular resonances for space debris orbits*, SIAM J. Appl. Dyn. Syst. 2016.

• A. Celletti, C. G., *A study of the lunisolar secular resonance* $2\dot{\omega} + \dot{\Omega} = 0$, Frontier in Astronomy and Space Sciences - Fundamental Astronomy, 2016.

• A. Celletti, C. Galeş, G. P. and A. Rosengren, *Analytical development of the lunisolar disturbing function and the critical inclination secular resonance*, Cel. Mech. Dyn. 2017.

• C. Lhotka, A. Celletti, C. G., *Poynting-Robertson drag and solar wind in the space debris problem*, Monthly Notices of the Royal Astronomical Society, vol. 460, 802-815, (2016).

• A. Celletti, C. Efthymiopoulos, F. Gachet, C. G. and G. Pucacco, *Dynamical models and the onset of chaos in space debris*, Int. J. Non-Linear Mech., 2017.

• A. Celletti, C.G.,*Dynamics of resonances and equilibria of low Earth objects*, SIAM Journal on Applied Dynamical Systems, 2018.